

Plasma Based Immuno-MRM Assays Against uPAR and Integrin $\alpha v \beta 6$ for Early Stage Colorectal Cancer Diagnosis

By
Sachini Fonseka

Submitted in accordance with the requirements for the degree of Masters in Research

Macquarie university
Faculty of Medical and Health Sciences

9th October 2017

ACKNOWLEDGEMENTS

I owe my deepest gratitude to my supervisor Prof. Mark Baker for his guidance and support towards the completion of the M.Res. thesis project "*Plasma Based Immuno-MRM Assays against uPAR and Integrin α v β 6 for Early Stage Colorectal Cancer Diagnosis*". I thank him for introducing me to the project which helped to learn multiple new skills such as immune-precipitation, proteomics and hands on training on mass-spectrometry. I would like to express my warmest regards to my co-supervisor Dr. Seong Beom Ahn. Without his continued guidance to perform experiments, this thesis would not have been possible.

I am deeply grateful to Dr. Mathew Mckay at Australian Proteomics Research Facility (APAF) who had been thoroughly involved in targeted proteomics experiments. His expertise, experience and guidance in troubleshooting and optimisation has been essential for completion of this work.

I would like to acknowledge help received from my colleague, a PhD student, Ms. Samridhi Sharma in fulfillment of this thesis. I thank Ms. Sharma for her time invested in discussion and optimisation necessary to define the protocols of the experiments and in development of a targeted assay. I would like to thank Mr. Subash Adhikari for providing his valuable assistance from time to time.

I finally also acknowledge support received from Dr. Seong Beom Ahn, Dr. Abidali Mohamedali, Ms Samridhi Sharma and Mr. Subash Adhikari in revision of thesis draft.

The acquisition of financial support for this project leading was received from departmental research funds from Faculty of Medicine and Health Sciences for M.Res. students and Cancer Council Australia grant awarded to Co-Supervisor Dr. Seong Beom Ahn.

Table of Contents

List of Abbreviations	4
Abstract.....	6
1. Introduction	7
2. Project Outline	17
3. Methods	17
3.1. Antibodies and recombinant proteins	17
3.2. Patient plasma samples	18
3.3. Determination of total protein in plasma samples.....	18
3.4. Western blotting analysis.....	19
3.5. Immunoprecipitation	20
3.6. Tryptic digestion and desalting of recombinant proteins and plasma samples	20
3.7. LC-PRM-MS analysis.....	21
3.8. HCT116 cell lysate preparation and LC-PRM-MS analysis	22
3.9. Data analysis	22
4. Results	23
4.1. Immunoaffinity enrichment.....	23
4.1.1. Determining mAb specificity.....	23
4.1.2. Determining antibody sensitivity	26
4.1.3. Protein A/G magnetic bead immunoprecipitation of recombinant $\beta 6$ protein.....	28
4.2. PRM Mass Spectrometry.....	30
4.2.1. uPAR product ion detection and intensity	30
4.2.2. uPAR transition limit of detection.....	36
5. Discussion	51
5.1. Affinity assays.....	51
5.1.1 Specificity and sensitivity assessment of antibodies	52
5.1.2. Immunoprecipitation of recombinant protein.....	53
5.2. PRM Mass Spectrometry.....	54
5.2.1. $\beta 6$ and uPAR product ion detection and intensity	54
5.2.2. $\beta 6$ and uPAR transition limit of detection.....	55
5.2.3. Transition evaluation and selection	57
5.2.4. The uPAR PRM assay validation in CRC cell lysate	59
5.3. Conclusion	61

List of Abbreviations

ABC	Ammonium bicarbonate
ACN	Acetonitrile
AJCC	American Joint Committee on Cancer
AS	Anti-sense
BCA	Bicinchoninic acid
BSA	Bovine serum albumin
Hb	Fecal haemoglobin
CEA	Carcinoembryonic antigen
CRC	Colorectal Cancer
DIA	Data independent acquisition
D1- 3	Domain 1-3
ECL	Enhanced chemiluminescence
ELISA	Enzyme-linked immunosorbent assay
FA	Formic acid
FOBT	Fecal occult blood test
FIT	Fecal immunochemical
GPI	Glycosyl phosphatidylinositol
IgG	Immunoglobulin
Immuno-MRM	Immunoaffinity target enrichment with multiple reaction monitoring
uPAR	Urokinase-type plasminogen activator receptor
uPA	Urokinase-type plasminogen activator
$\alpha\beta 6$	Integrin alpha v beta 6
ECM	Extracellular matrix
EMT	Epithelial-mesenchymal- transition
LAPs	Low abundant proteins
LC	Liquid Chromatography
LOD	Limit of detection
mAb	Monoclonal antibody
MARS14	Agilent 14 multiple affinity removal column
MS	Mass spectrometry

MRM	Multiple reaction monitoring
MMP	Matrix metalloprotease
MW	Molecular weight
m/z	Mass to charge ratio
NHS	N-Hydroxysuccinimide
PRM	Parallel reaction monitoring
prEST	protein epitope signature tag antibody
SDS-PAGE	Sodium dodecyl sulfate polyacrylamide gel electrophoresis
SEM	Standard error of mean
IP	Immunoprecipitation
TGF- β	Transforming growth factor beta 1
WB	Western blot
WT	Wild type
QQQ	Triple quadrupole MS instrument

Abstract

Colorectal cancer (CRC), characterised by tumours of the colon, rectum and appendix, is the 3rd leading cause of cancer-related death worldwide. The survival rate is dependent on the time of diagnosis, with early-stage detection leading to curative surgical resection. Despite this, a lack of accurate, sensitive and specific tests means that only ~30% of cases are diagnosed early enough to be cured (i.e., AJCC Stages I & II). To address this unmet clinical need, this thesis addressed developing a mass spectrometry (MS)-based assay for the detection and quantification of early-stage blood-based biomarkers of CRC. Here, we have developed targeted assays for the potential cancer biomarkers urokinase plasminogen activator receptor (uPAR) and integrin $\alpha\text{v}\beta\text{6}$. A growing portfolio of evidence implicates both proteins as important regulators of the epithelial-mesenchymal transition (EMT), a mechanism known to be critical in cancer proliferation, progression, invasion and eventual metastasis. The biggest challenge in detection and quantification of these biomarkers in plasma is their relatively low abundance (low ng/mL) compared to more highly abundant homeostatic proteins (high mg/mL). To circumvent this challenge, we developed a two-step assay that captures the proteins by affinity-based enrichment prior to quantitation by targeted multiple reaction monitoring (MRM) MS. Initial studies were aimed at determining the specificities of a range of monoclonal antibodies for their intended target. Subsequent studies using a surrogate parallel reaction monitoring (PRM)-MS established optimal peptide transitions, as well as each assay's limits of detection. Collectively, the amalgamation of these two components (with the use of labelled peptide standards) will result in highly sensitive, specific and reproducible assays to detect and quantify uPAR and $\alpha\text{v}\beta\text{6}$ in control and diseased patient plasma. Early stage diagnosis will shift the percentage of CRCs detected towards the localized tumour stages (I and II), with consequential increased patient survival.

1. Introduction

1.1. Colorectal cancer

Colorectal cancer (CRC), characterized by tumours of the colon, rectum and appendix, is the 3rd leading cause of cancer related death worldwide. Globally, there are 1.4 million new diagnoses and 694,000 deaths every year [2]. As with many cancers, the survival rate is dependent on the stage of diagnosis. With CRC, surgical resection is near curative, with a 90% survival rate, if the tumour is detected early (i.e., AJCC stage I/II) [3]. However, a lack of early detection means only 9% of cases are diagnosed at stage I and 24% at stage II [4]. The ~70% majority are diagnosed at stages III, IV where tumours have become invasive and thus often require additional treatment. Patients diagnosed with late stage (III/IV) tumours have a poor 5-year survival rate of <10% [5]. Early detection and prediction with accurate treatment can possibly combat this mortality rate.

The most routinely used method in CRC screening relies upon the presence of fecal haemoglobin (Hb), detected chemically (fecal occult blood test: FOBT) or immunologically (fecal immunochemical: FIT) [6]. Whilst relatively sensitive, these tests are not very specific due to benign conditions such as rectal tears also releasing Hb [7]. A positive result in these tests is often followed up by a direct structural examination such as a colonoscopy or sigmoidoscopy, which has high sensitivity and specificity [8]. However patient reluctance in faeces handling reduces screening adherence, with only 60% of eligible adults participating [9].

Given the promising survival rate with early detection, global research efforts are focused on developing early stage-specific diagnostic tests. These need to be more sensitive and specific at detecting early stage CRCs compared to the FOBT/FIT and limit the co-morbidities associated with unnecessary colonoscopies. Additionally, to avoid the potential discomfort and difficulty in stool testing, a diagnostic blood test is particularly attractive [10]. Such a blood test could potentially be designed to measure proteins released from tumour cells.

1.2. Cancer Biomarkers

The National Cancer Institute defines a biomarker as a “biological *molecule found in the blood, or other body fluids, or tissue that is a sign of a normal or abnormal process, or of a condition or disease*” [11] (National Cancer Institute, 2012). Disease biomarkers can be used to detect disease, predict drug response and/or recurrence. Advances in genomics and proteomics have highlighted a plethora of diverse molecular pathways that can be targeted in CRC diagnosis [12].

Currently, the only clinically available serum protein biomarker for CRC is the carcinoembryonic antigen (CEA). Its endogenous expression is limited to fetal development however elevated levels are found in certain cancers including CRC [13]. Other benign factors such as heavy smoking and diabetes mellitus also elevate CEA levels, which reduces its specificity in identifying CRC [14, 15]. Measurement of CEA levels in plasma is used in clinical practice as a follow up tool after surgical resection to predict CRC recurrence. However, it is plagued by low sensitivity (64%) that limits its use to a first-line surveillance investigation that needs to be supplemented with clinical, radiological and/or histological confirmation [16-18]. It is worth noting, that CEA does not delineate early stage CRC (Zhu et al., 2015). More recently, a blood test has been developed to test CRC recurrence, claiming greater sensitivity than the CEA test [19]. The Colvera™ test is currently under clinical trial in Australia and is based on measuring circulating tumour DNA in post-surgery patients blood to predict recurrence [20]. Whilst this is a remarkable success in CRC research an improved strategy for early stage detection is still missing.

Key mechanisms driving tumour malignancy are potential targets for early stage detection. Specifically, the epithelial-mesenchymal-transition (EMT), TGF- β activation, extracellular matrix remodeling, elevated cell proliferation, increased migration and invasion are some of the pivotal processes by which epithelial tumours become malignant [21]. Core proteins associated with these processes are intuitive candidates for early stage-specific biomarkers. We have discovered a membrane protein-protein interaction that is critical to CRC malignancy: the receptor urokinase plasminogen activator receptor (uPAR) and integrin alpha v beta 6 ($\alpha v\beta 6$) [22].

1.3. The urokinase plasminogen activator receptor in CRC

The intricate cell-extracellular matrix (ECM) crosstalk is crucial during development as well as normal function during adult life, and is mediated through plasma membrane receptors such as uPAR. Altered ECM receptors expression and regulation occurs in several human diseases including cancer and such changes contribute to maladaptive adhesion properties, and aberrant cell signaling to drive tumour progression [1]. One important requirement of cell invasion is coordinated ECM proteolysis.

The regulation of the plasminogen activation system, an extracellular proteolytic cascade, is carried out primarily by the urokinase plasminogen activating receptor (uPAR) (Figure 1). A glycosyl phosphatidylinositol (GPI) linker anchors the three domains (D1, D2, D3) of the protein to the external surface of the plasma membrane [23]. It localizes the serine protease urokinase-type plasminogen activator (uPA) for an extracellular proteolytic cascade [24]. In a positive feedback loop, activated uPA cleaves plasminogen to create the protease plasmin which in turn cleaves and activates pro-uPAR [25]. This process is amplified by the level of uPAR interactors at the cell surface [26]. Plasmin drives ECM proteolysis via degradation of its components and activates matrix metalloproteinases (MMPs), cytokines and promotes angiogenesis, [27-29]. Increased plasmin activity via increased uPAR expression facilitates cancer cell motility by degradation of the ECM structures. Additionally, plasmin and MMPs can release ECM-bound growth factors or activate latent growth factors to further promote cell growth [30, 31]. Cancer cell escape and potential secondary colonization are crucial in tumour metastasis.

Homeostatic expression of uPAR is fairly limited with elevation found in ECM remodeling conditions such as gestational tissues during development, keratinocytes during wound healing and in stress, injury and inflammatory conditions [32, 33]. For example, expression can be detected in the central nervous system following ischaemia [34]. There is considerable evidence of uPAR expression in many epithelial cancers including CRC. In line with its role in cell motility, expression in CRC tumour cells is characteristically restricted to the invasive edge [35]. There is a tight correlation between high uPAR expression and poor patient prognosis [1, 36, 37]. Importantly, expression in

CRC appears to increase with severity, notably during the transition to an invasive carcinoma (Suzuki et al., 1998). The report of a change in magnitude of uPAR expression between stage II and III rectal cancer tissue is extremely promising [38]. Differentiating between these stages would enable detection before cancer metastasizes and thus direct efficient surgery based treatment. However, this study was in tissue samples and is yet to be translated to uPAR in plasma which would be required for a blood based diagnostic test.

Phospholipase [39] and extracellular proteolytic cleavage [40] of the GPI anchor releases soluble uPAR into the blood. Full length (D1-D3) and all three of its domains have been identified in biological fluids [41-43]. The prognostic utility of uPAR has been explored using tumour tissue extracts and plasma. A study of pre-and post-operative CRC stage B plasma revealed that soluble uPAR, as measured in an enzyme-linked immunosorbent assay (ELISA), above and below a median cut off point can differentiate patients with poorer survival [44]. This indicates soluble uPAR as an independent prognostic marker that could differentiate stage B cancers that are surgically curative against those which relapses.

Whilst there is evidence of soluble uPAR to be significantly higher in CRC patients compared to healthy controls [45] its diagnostic potential is yet to be fully explored. Therefore, we aim to develop an assay to detect and quantify uPAR in CRC plasma to detect early stage tumours.

Independent of its role in the extracellular proteolytic cascade uPAR has also been shown to be a signaling receptor driving cancer cell characteristics of invasion, proliferation and survival (Figure 1). Due to lack of a transmembrane and an intracellular domain, uPAR requires interaction with ligands such as transmembrane receptors for cell signaling. The integrin family of receptors are considered the major co-receptors of uPAR [46].

1.4. Integrin $\alpha\beta6$ in CRC

One of uPAR's integrin co-receptors is the epithelial restricted integrin $\alpha\beta6$. Our group inferred their interaction by co-immunoprecipitation of uPAR and $\alpha\beta6$ from a

human ovarian cancer cell line [47]. Furthermore, their precise binding sites were elucidated by a peptide array containing linearized uPAR, proximity ligation assay [22] and in silico structural modelling [48]. The β_6 subunit of the $\alpha v\beta_6$ integrin is epithelial restricted with minimal homeostatic expression, detected only under wound healing conditions and in tumour islands [49, 50]. It is a transmembrane receptor composed of non-covalently linked αv and β_6 , where the β_6 subunit partners exclusively with αv to form a single heterodimer [51]. The $\alpha v\beta_6$ signals through its C-terminal cytoplasmic sequence to activate the Extracellular Signal Regulated Kinase (ERK)/ Mitogen Activated Protein Kinase (MAPK) pathway, which is elevated in CRC metastasis [47, 52]. Cell migration inhibition in β_6 knockout cells implies its crucial role in cell motility (Huang et al., 1998). Immunological based methods have repeatedly detected increased levels of $\alpha v\beta_6$ in various epithelial cancers and is often correlated to invasion and poor prognosis [53-55]. Promotion of cell invasion and migration are both aspects of metastasis and thus $\alpha v\beta_6$ is considered a regulator of tumour metastasis.

In colon cancer, $\alpha v\beta_6$ expression is concentrated to the leading edge of tumours and is accompanied with EMT phenotypes and also elevated MMP9 [56]. MMP9 is a marker of cell motility, given its function in degrading the basement membrane required to restrain migratory cells [57]. Additionally, many lines of evidence point to the activation of transforming growth factor beta (TGF- β), a recognised EMT inducer, as an important pathway in $\alpha v\beta_6$ signaling [58]. In colon cancer models, increased $\alpha v\beta_6$ expression coincides with TGF- β activation whereas antibody mediated inhibition of $\alpha v\beta_6$ activation of TGF- β suppresses EMT [47, 59].

In addition to its diagnostic potential $\alpha v\beta_6$ expression in cancer can also be exploited in adjuvant chemotherapy. Liang et al., used its restricted cancer cell expression for drug delivery. They developed targeted immunoliposomes conjugated to $\alpha v\beta_6$ monoclonal antibodies, to deliver 5-fluorouracil to achieve increased cancer cell apoptosis compared to non-targeted liposomes [60]. There is striking evidence that elevated $\alpha v\beta_6$ expression in early stage (I or II) tumours have a significant 28% reduction in the 5-year survival rate compared to patients with low or no $\alpha v\beta_6$ expression [55]. Scharl and colleagues [61] used an ELISA to detect B6 in CRC patient plasma to discover a cut off value of 4ng/mL B6. Higher serum levels were associated with 100% metastasis and

poorer survival. The authors followed on a with a patent to use $\alpha\beta6$ for diagnosis/prognosis of CRC using an ELISA method [62]. Therefore, we predict $\alpha\beta6$ to be an independent prognostic variable that can predict survival outcome at early stage CRC. The evidence of $\beta6$ and uPAR release in to plasma makes them ideal targets for a blood based assay.

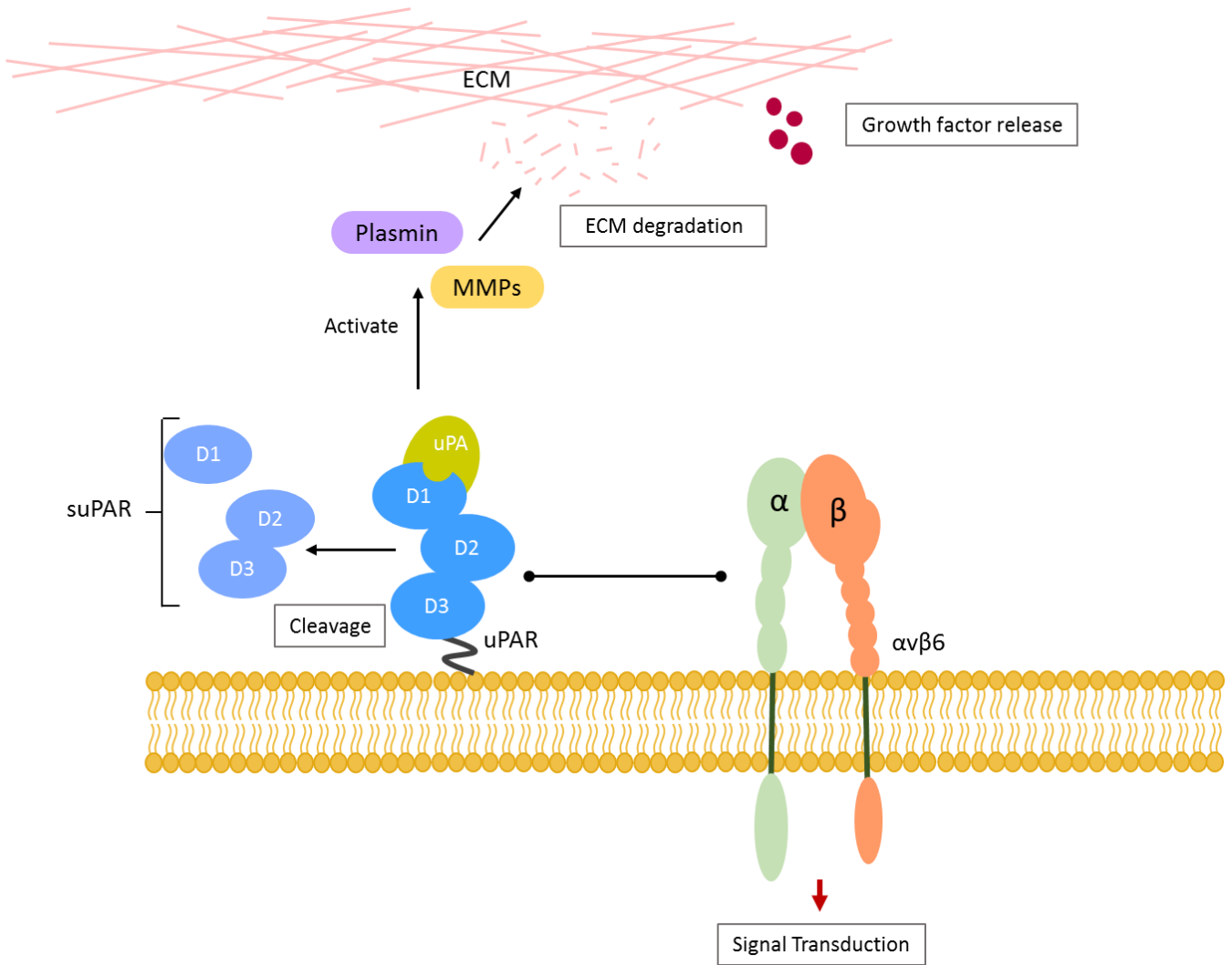


Figure 1. The role of uPAR and $\alpha\beta6$ in cancer. The GPI anchored receptor, uPAR, binds the protease uPA at the extracellular plasma membrane to generate the active protease plasmin. Plasmin activates matrix MMPs and both act to degrade extracellular matrix (ECM) components and release growth factors from ECM sequestration. Complexes of uPAR and its ligands co-interacts with the integrin $\alpha\beta6$ for intracellular transduction. The C terminal end of $\beta6$ signals various cancer cell hallmark mechanisms such as TGF- β activation, proliferation and survival. Adapted from Smith and Marshall [1].

1.5. The Plasma Proteome

The plasma proteome is one of the most complex proteomes in the human body as it contains more than 10,000 diverse proteins [63]. This complexity and wide dynamic range in protein concentration is a challenge for biomarker detection [64]. Currently, the most common approaches in plasma proteomics are gel based applications, chromatography, western blot assays (WB), enzyme-linked immunosorbent assays, immunoprecipitation (IP) and mass spectrometry (MS). MS is an analytical technique that identifies proteins by separation based on mass to charge ratio (m/z) and is the powerhouse of proteomics, due to its highly precise and high throughput nature [65].

The biggest challenge in plasma biomarker discovery and quantification is the wide dynamic range of protein concentration in human plasma, ranging from milligrams to less than picograms per millilitre (13 orders of magnitude). For example, we know that liver-derived proteins (e.g. human serum albumin, mg/ml level) are highly abundant, and that it interferes with the detection and quantification of low abundant proteins (LAPs) such as uPAR and $\alpha\beta6$ (found at low ng/ml levels) [63].

To overcome this dynamic range, plasma samples are generally depleted of the high abundant proteins before introducing into the MS sample preparation workflow. An example is the commercially available Agilent 14 multiple affinity removal column (MARS-14), which uses 14 high specificity antibodies to deplete the top 14 abundant proteins from plasma [66]. Another alternative to depletion would be an immune-based targeted approach. In this method, target/protein of interest is captured immunogenically and introduced into highly sensitive targeted MS to facilitate detection of low abundant proteins [67].

1.6. Immunoaffinity enrichment coupled multiple reaction monitoring

The amalgamation of immunoaffinity target enrichment with multiple reaction monitoring (MRM) termed immuno-MRM offers an advantageous tool for target identification and quantification in a complex biological sample such as plasma. Immuno-MRM relies on the principle of up-front target enrichment, and targeted mass selection/s

in a specialized triple quadrupole (QQQ) MS instrument (e.g., SCIEX QTRAP™ 5500).

MRM is an established technique for the precise and specific quantitative analysis of protein expression. It is a targeted MS/MS technique that can be used to filter peptides of interest by their m/z . The 1st quadrupole (first mass analyser) is designed to select a peptide of particular m/z for subsequent fragmentation in the 2nd quadrupole (collision cell) and the 3rd quadrupole (second mass analyser) is designed to select a fragment/daughter/product ion of particular m/z for detection [68]. This peptide and fragment ion pair is termed a transition and multiple reliable transitions establish the identification and subsequent quantification of a target protein. Assay development requires selection and optimization of multiple reliable transitions per peptide. Whilst MRM is a powerful tool for detection and quantification it is constrained by sample complexity. Several studies indicate the need for very extensive fractionation to detect and quantify proteins at concentrations lower than 1 $\mu\text{g/ml}$ in plasma [69, 70].

Antibody-mediated protein enrichment/capture prior to MRM is a key advantage as it potentially overcomes the problem of low abundant targets. Specifically, the target protein is captured out of the complex plasma sample by an antibody in an immunoprecipitation experiment. MRM sensitivity is enhanced up to 10^4 fold by coupling it to an upstream immuno-enrichment phase, thus the antibodies effective capture is a critical point [67]. Antibody validation is a requirement for immune assay development and is defined as proof of specificity, sensitivity and reproducibility [71]. Specificity is the accuracy of the antibody in targeting its antigen (minimal cross-reactivity) and sensitivity is the limit of detection (LOD, lowest amount of antigen detectable). Plasma with its dynamic range and complexity requires antibodies with high specificity and sensitivity. Protein conformation, target accessibility and the ratio of target to off-target proteins all effect antibody performance. Thus, validation needs to be carried out in an application- and context- specific manner. Whilst rigorous testing is time consuming the successful validation of a commercial antibody for immuno-MRM is highly advantageous, as it establishes the use of existing, readily-available reagents which can be standardized across laboratories [72].

Following the validation of antibodies and establishment of transitions, the assay

can be designed for quantification. Addition of specific quantities of isotopically-labelled synthetic (i.e., heavy) homolog peptides enables precise absolute quantification. The ratio of heavy to light peptide is used for the quantification [67]. MRM quantitative analysis is reported to have very low coefficients of variation and high reproducibility and is considered the most sensitive strategy for protein detection [73]. Once the parameters of identification and quantification are established, it constitutes a definitive assay that can be perpetually used to detect and quantify those specific targets. Hoofnagle and colleagues demonstrated the quantification of plasma thyroglobulin using immunoaffinity enrichment coupled to MS at a picomolar limit of detection whilst avoiding endogenous immunoglobulin interference so frequent in traditional immunoassays (Hoofnagle et al., 2008). Furthermore, several groups have successfully utilised immuno-MRMs to assay other plasma LAPs [74-79].

Some of the advantages of multiplexed immuno-MRM are that it is highly targeted, reduces interference by background components and greatly enhances sensitivity [72, 80]. The multiplexing capability of immuno-MRM facilitates the development of MRMs for a panel of biomarkers able to assess multiple disease characteristics, such as differentiating early to late stage CRC.

Whilst both uPAR and to a lesser extent $\alpha\beta6$ have been quantified in plasma using traditional ELISA based methods, it remains to be targeted via MS. Given the advantages of high specificity, multiplexing, standardization and high inter-laboratory reproducibility in an immune-MRM, here it is proposed as a highly suitable strategy to accurately quantify biomarkers in plasma [81, 82]. An immuno-MRM assay able to detect and quantify CRC blood based biomarkers $\alpha\beta6$ and uPAR has potential to be utilised across laboratories and clinical settings to measure tumour stage and progression [83].

One of the main challenges in designing a MRM assay is its laborious optimization. But the development of sensitive orbitrap based (e.g. Thermo Scientific™ Q-Exactive™ Hybrid Quadrupole-Orbitrap) instruments and a technique described by Coon's lab can aid to reduce this time consumption. The Q-Exactive is a hybrid quadrupole-orbitrap instrument which delivers exceptional performance through a combination of quadruple precursor ion selection and high-resolution, accurate-mass (HRAM) Orbitrap detection of all daughter

ions. Coon and colleagues suggested using this instrument in a technique referred to as ‘parallel reaction monitoring’, or PRM [84]. Unlike in a typical MRM where each peptide has one daughter ion monitored at a time in PRM mode on the Q-Exactive, all the daughter ions could be detected in parallel in a single analysis. This method can be utilized to reduce the optimization required for a MRM assay. Initial experiments in PRM monitoring of all transitions will allow selection of best performing transitions.

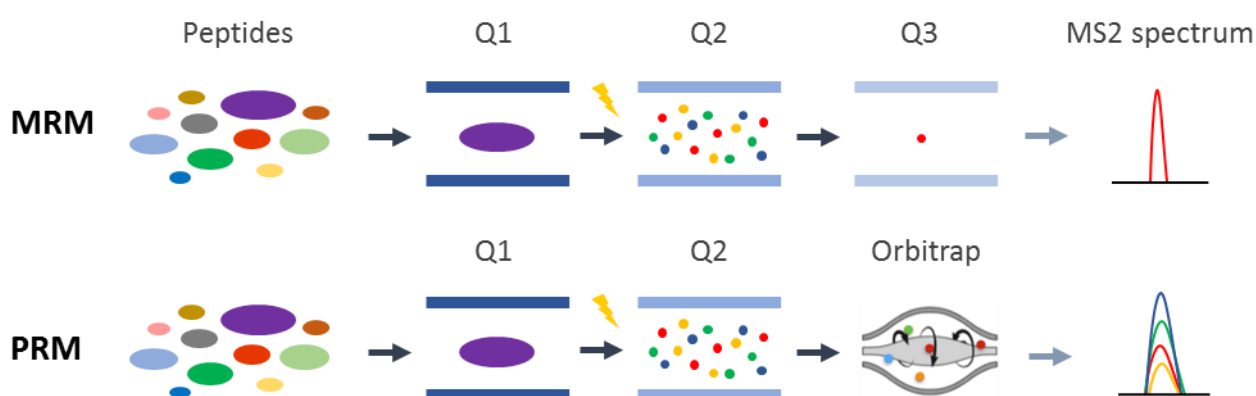


Figure 2. Comparison of multiple reaction monitoring (MRM) and parallel reaction monitoring (PRM) mass spectrometry (MS). In both PRM and MRM-MS, in the first quadrupole (Q1) a peptide of specific mass is selected for subsequent fragmentation in the collision cell (Q2). In the 3rd quadrupole, of an MRM MS (e.g. triple quadrupole MS; AB Sciex 5500+) a single daughter ion for each peptide is selected for detection. Whereas in an PRM MS (e.g. Hybrid Quadrupole-Orbitrap MS; Thermo Q Exactive™) the Orbitrap does a full high-resolution scan of all the daughter ions from a peptide. Therefore, in an MRM experiment a single daughter ion for each peptide is monitored (MS2 spectrum) whereas in an PRM all the resulting daughter ions are monitored.

2. Project Outline

This project aimed to develop immuno-MRM assays for the early stage CRC biomarkers uPAR and $\alpha\beta 6$. Focus was on the two main components of the assay: (1) immunocapture of target in plasma and (2) MRM detection. The affinity-based capture of targets required a comprehensive analysis of antibody specificity and sensitivity. Following this, a successful immunoprecipitation strategy was developed. In contrast, the MRM optimization focused on the accurate detection of $\beta 6$ and uPAR peptides. A surrogate PRM-MS analysis was used to determine the transition performance, linearity and limit of detection. Lastly, the uPAR PRM assay was successfully validated using a stage B CRC cell line.

3. Methods

3.1. Antibodies and recombinant proteins

The combination of plasma and recombinant proteins was used as a model of CRC plasma to develop the immuno-MRM assay. Recombinant human $\alpha\beta 6$ protein (R&D #3817-AV-050) is Chinese hamster ovary cell line derived and composed of non-covalently linked α (110.5 kDa) and $\beta 6$ (68.6 kDa) in a 1:1 ratio. SDS-PAGE under reduced conditions predicted molecular masses are 145 kDa (α) and 115 kDa ($\beta 6$). Recombinant human uPAR protein (R&D #807-UK/CF-100) is mouse myeloma cell line derived, with a predicted molar mass of 40-55 kDa under reduced conditions.

The monoclonal antibodies (mAbs) against the $\beta 6$ subunit of $\alpha\beta 6$ were collaboratively provided from Biogen Idec, Cambridge [85] (Table 1). In addition, mAb Hupo8 which is a protein epitope signature tag (prEST) antibody was developed in collaboration with the Human Protein Atlas to target the EVLGDTEGLNLSFTAICNNGTLFQ HQKKCSHMKVGDTASFSVTVNIPHERRSRHIIKPVGLGDALELLVSPECNDCQKEVEVNSSKCHHG N sequence of $\beta 6$. The uPAR mAbs were purchased from Seksui in addition to in-house developed mAb Mab1 which is targeting uPAR D1D2 linker sequence (Table 1). Immunoglobulin isotype control antibodies (IgG1 and IgG2) and anti-mouse horse radish peroxidase-conjugated secondary antibodies (2° Ab) were purchased from R&D systems.

Table 1. List of tested β 6 and uPAR antibodies

Antigen	Antibody	Host	Isotype	Manufacturer
β6	mAb 6.3G9	Murine	IgG1	Biogen
	mAb 6.2A1	Murine	IgG1	Biogen
	mAb 6.4B4	Murine	IgG1	Biogen
	mAb Hu8G6	Murine	IgG1	Biogen
	mAb Hupo8	Murine	IgG2a	In house
	mAb 7.8B3	Murine	IgG1	Biogen
uPAR	mAb 3937	Murine	IgG1	Seksui
	mAb 3936	Murine	IgG2a	Seksui
	mAb R4	Murine	IgG1	Seksui
	mAb Mab1	Murine	IgG1	In house

3.2. Patient plasma samples

Control human plasma samples were obtained under a collaborative project with Prof. Gilles Guillemin (HREC Ref #5201600401 and #5201700681). Samples were collected from an age and gender-matched healthy (non-CRC or similar epithelial cancer) cohort.

3.3. Determination of total protein in plasma samples

Plasma protein concentration was determined by a bicinchoninic acid (BCA) assay kit (Pierce™ #23225) according to the manufacturer's protocol. The bovine serum albumin (BSA) standards were prepared by serial dilution of known BSA concentration. Plasma (diluted 10-fold) and standard samples (25 μ l) were incubated with pre-mixed working reagent (50:1 mixture of reagent A and B) for 30 min at 37°C in a 96 well plate (Sigma #CLS3340). The absorbance at 562 nm was measured by a spectrophotometer (PHERAstar FSX) and a standard curve constructed to determine the plasma protein concentration.

3.4. Western blotting analysis

3.4.1. Specificity assay

All mAbs were tested for specificity against its respective recombinant target protein in a plasma background, via a western blot analysis. The samples were recombinant protein only (1 μ g), plasma proteins (25 μ g), and mixture of recombinant (1 μ g) and plasma proteins (25 μ g). Proteins were mixed with TruPAGE LDS™ sample buffer (Sigma-Aldrich #PCG3009) and reducing agent (Sigma-Aldrich # PCG3005), denatured at 95°C for 5 mins followed by micro-centrifuge at 12,000 rpm for 1 min prior to loading into the SDS-PAGE. Proteins were separated on 4-12%, or 12% polyacrylamide gels (Sigma-Aldrich #PCG2006), at 200 volts for 45-60 min. Gels were transferred onto a nitrocellulose membrane (BIO-RAD, Trans-Blot Turbo Transfer system). Membranes were incubated in Ponceau S solution (Sigma #P7170) for 3 min and image developed (BIO-RAD, ChemiDoc XRS+) with automatic exposure for most intense bands. The Ponceau stain was used as a loading control to assess equal protein loading [86]. Membranes were blocked by 5% non-fat milk powder dissolved in Tris-Buffered saline with 0.1% Tween 20 (TBST, pH 7.6) for 1 hr, and then incubated overnight at 4°C in primary mAbs as listed in Table 1, at a concentration of 1 μ g/mL. After 3, 5 min washes with TBST, membranes were incubated with peroxidase-rabbit polyclonal secondary antibody to mouse IgG (Sigma-Aldrich #A9044) for 2 hrs at room temperature at a concentration of 1 μ g/mL. After 3, 5min TBST washes and 2, 5min TBS washes membranes were incubated in enhanced chemiluminescence (ECL) kit reagents (BIO-RAD, Clarity Western ECL Blotting Substrates) and imaged for the highest intensity bands. Image Lab™ Software (BIO-RAD) was used for acquisition and analysis.

3.4.2. Sensitivity Assay

The mAbs that showed convincing results from the specificity analysis were then tested for sensitivity. This was accomplished by spiking in 500, 100, 10 and 1 ng of recombinant protein into 25 μ g of plasma. The SDS-PAGE and western blot was developed as detailed above.

3.5. Immunoprecipitation

Recombinant uPAR and $\alpha\beta6$ protein immunoprecipitation (IP) was performed by two independent methods: Pierce Direct Magnetic IP Kit (CAT#88828) and Protein A/G magnetic beads (Genscript #L00277).

The Pierce Direct Magnetic IP Kit utilizes the N-Hydroxysuccinimide (NHS) chemistry to covalently immobilize the antibodies to magnetic beads and was used according to the manufacturer's directions. Beads were activated with ice-cold 1 mM hydrochloric acid and incubated with the mAb for 60 mins at room temperature. The linking reaction was quenched with borate buffer (supplied in the kit) and beads incubated with the antigen for 2 hrs at room temperature. A magnetic rack was used to collect the beads and proteins were eluted with a low pH~2 glycine shock. The eluate and supernatants were probed with the same antibody used in the IP, on a western blot for validation. The protocol was tested with all available antibodies (1 μ g) to capture its recombinant protein (1 μ g) target.

The Protein A/G magnetic bead protocol relies on the affinity of protein A/G to antibody IgG [87]. Antibody and target protein was incubated in 0.5 mL of IP buffer (0.025 M Tris, 0.15 M NaCl, 0.001 M EDTA, 1% NP40, 5% glycerol, pH 7.4) overnight on a rotator at 4 °C. The following day 50 μ L of homogenized bead slurry was added and the mixture was rotated for 2 hrs at 4 °C. A magnetic rack was used to collect the beads and supernatant collected for analysis. Samples were eluted in TruPAGE LDS™ sample buffer at 95 °C for 5 mins. A fraction of the eluate and supernatant was processed for the western blot as described above. The western blot was probed using the same antibody as used in the IP. Negative controls were an IP with the antibody alone, recombinant protein alone and a positive control on the SDS-PAGE was 1ug of recombinant protein.

3.6. Tryptic digestion and desalting of recombinant proteins and plasma samples

All recombinant, plasma and cell lysates were prepared for mass spectrometry analysis using the following protocol. First, proteins were reduced to final 5 mM dithiothreitol (BIO-RAD, #1610611) for 30 mins at 55 °C and cooled before being alkylated to final 14 mM iodoacetamide (BIO-RAD, #1632109) for 30 mins at room temperature in the dark. Samples

were brought to pH~8 with serial additions of 1 M ammonium bicarbonate (ABC). Trypsin was used to digest the samples at a ratio of 1:30 to protein mass and was performed overnight at 37 °C. Following digestion, the samples were acidified to pH~2.5 using 1% formic acid (FA) to stop trypsin activity and mediate binding to C18 and desalted by Micro-C₁₈ Zip-Tip (MERK #ZTC18S096). All solutions used were MS grade, and the experiment was performed on low-bind tubes. Zip-Tip was activated with 3 washes of 100% acetonitrile (ACN), followed by 5 washes with 0.1% FA. Peptides were loaded to Zip-Tip by multiple pipetting, and washed 6 times by 0.1 % FA. Finally, peptides were eluted with 10 µL of elution buffer composed of 80% ACN and 0.1% FA in water.

The 2 µg binding capacity of the Micro-C₁₈ Zip-Tip was taken as the final peptide recovery. Samples were dried in a Vacuum Concentrator Plus (Eppendorf #5305000304) and resuspended in 0.1% FA. The samples were then micro-centrifuged at 12,000 g for 15 min at 4 °C before transferring 10 µL into total recovery MS vial (Waters # 600000750CV).

3.7. LC-PRM-MS analysis

A nano liquid chromatography (LC) system (Thermo) equipped with a column packed with Michrom Magic C18 (75 µm x 15 cm, 5 µm, 120 Å) was used to separate peptides. Samples (10 µL) were injected into the column in 99% buffer A (0.1% FA) and 1% buffer B (0.1% FA in ACN). Samples were separated at a flow rate of 0.3 µL/min with a 50 mins linear gradient from 1% to 65% buffer B, a 2 mins linear gradient from 65% to 85% buffer B, and a final 8 mins gradient from at 85% buffer B. Blanks were run between each complex sample (i.e., lysate), and every 3rd recombinant sample. The blanks were separated at a flow rate of 0.3 µL/min with a 30 mins linear gradient from 1% to 50% buffer B, a 2 min linear gradient from 50% to 85% buffer B, and a final 8 mins gradient from at 85% buffer B. The resolved fractions were applied to an Thermo Scientific™ Q-Exactive™ Hybrid Quadrupole-Orbitrap Mass Spectrometer with a nano-electrospray ionization source. The PRM method was modified for a resolving power of 17,500 at 200 m/z, isolation window of 2.0 m/z and normalized collision energy of 30%. PRM acquisition methods were constructed using inclusion lists obtained from SRMATlas and in-house data independent acquisition (DIA) experiments. The inclusion list was determined by searching SRMATlas for the top ~10 peptides per protein constraint.

3.8. HCT116 cell lysate preparation and LC-PRM-MS analysis

Wild type (WT) HCT116 is a CRC tumour stage B derived cell line with known expression of uPAR (Ahmed et al., 2003). The anti-sense cell line (AS) has a stable transfection of uPAR-siRNA that produces a 27% knock down of uPAR protein [88]. These two cell lines were used to test the specificity and sensitivity of the PRM assay. The lysates were kindly donated by Dr. Charlie Ahn for analysis. Cells were lysed with 0.1 % sodium deoxycholate and 100 mM triethylammonium bicarbonate buffer and protein concentration determined via BCA assay and duplicate samples processed for MS as described above. The estimated maximum load on a nano-LC column (2 µg of each sample) was injected into the LC-PRM-MS and analysed for all uPAR transitions. Due to the complexity of the lysate more manual adjustment in Skyline was required. The peak boundaries were adjusted for the ions with repeated retention times across all samples. Representative peaks are in supplementary information (Figure 11).

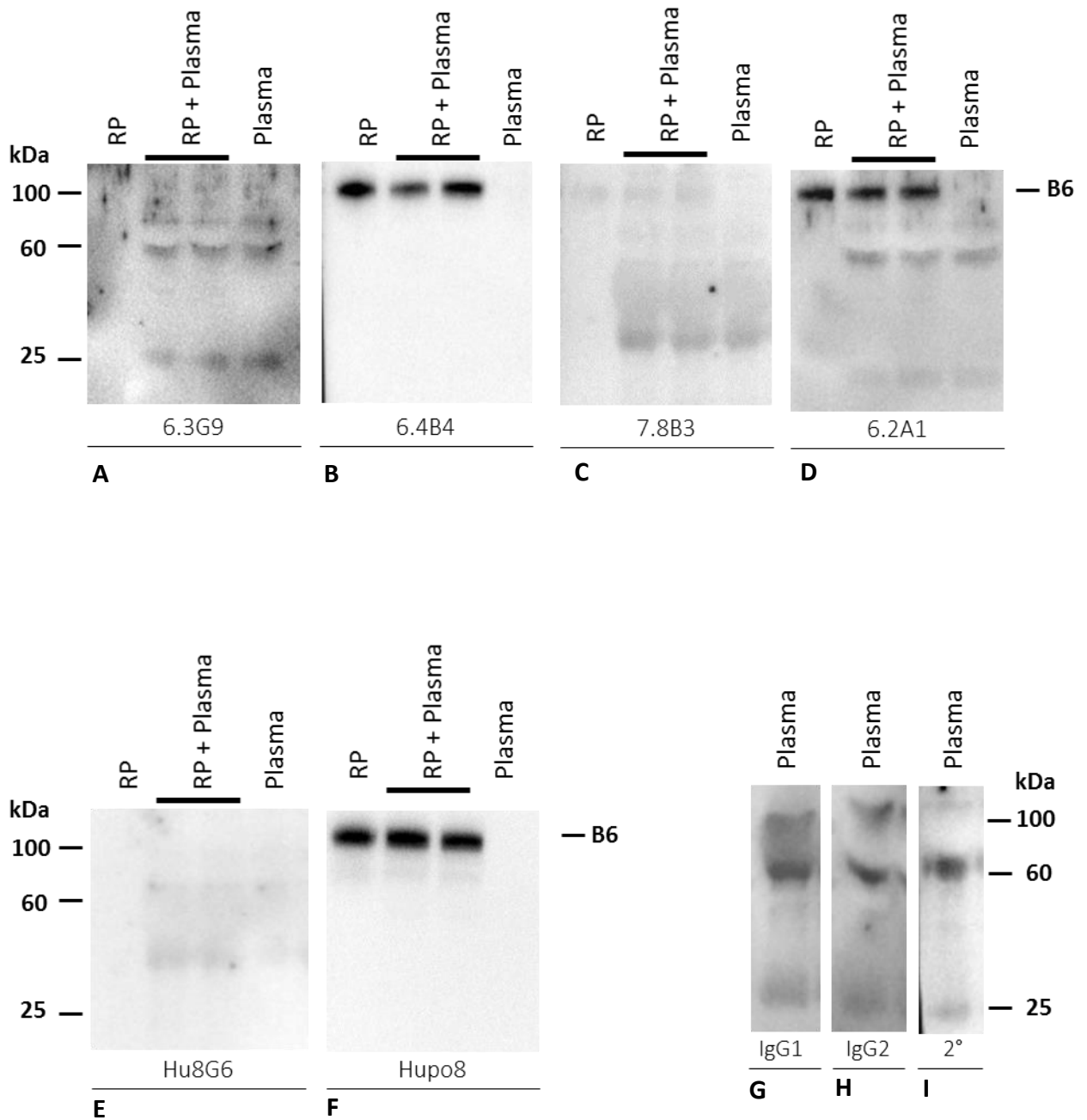
3.9. Data analysis

The molecular weight (MW) of bands in the western blot was measured using relative migration distance. The distance travelled by ladder protein standards were divided over total migration distance as determined by the Coomassie blue end and a standard curve made with LogMW. The bands of interest were measured and MW determined using the linear equation of the standard curve. All raw MS data were processed using Skyline software [89] programmed with the mass list of peptides used in PRM acquisition. Peak integration was performed automatically by the software, with exceptions noted, and also manually inspected. Search parameters were set to identify singly and doubly charged y and b-ions. Where appropriate outlying data points were excluded from response curves. An unpaired T-test was used to compare transitions in recombinant and cell lysate experiments. Two linear regression models (described in detail later) were used to analyse the concentration and peak response curves, using GraphPad Prism software (version Prism 7).

4. Results

4.1. Immunoaffinity enrichment

4.1.1. Determining mAb specificity



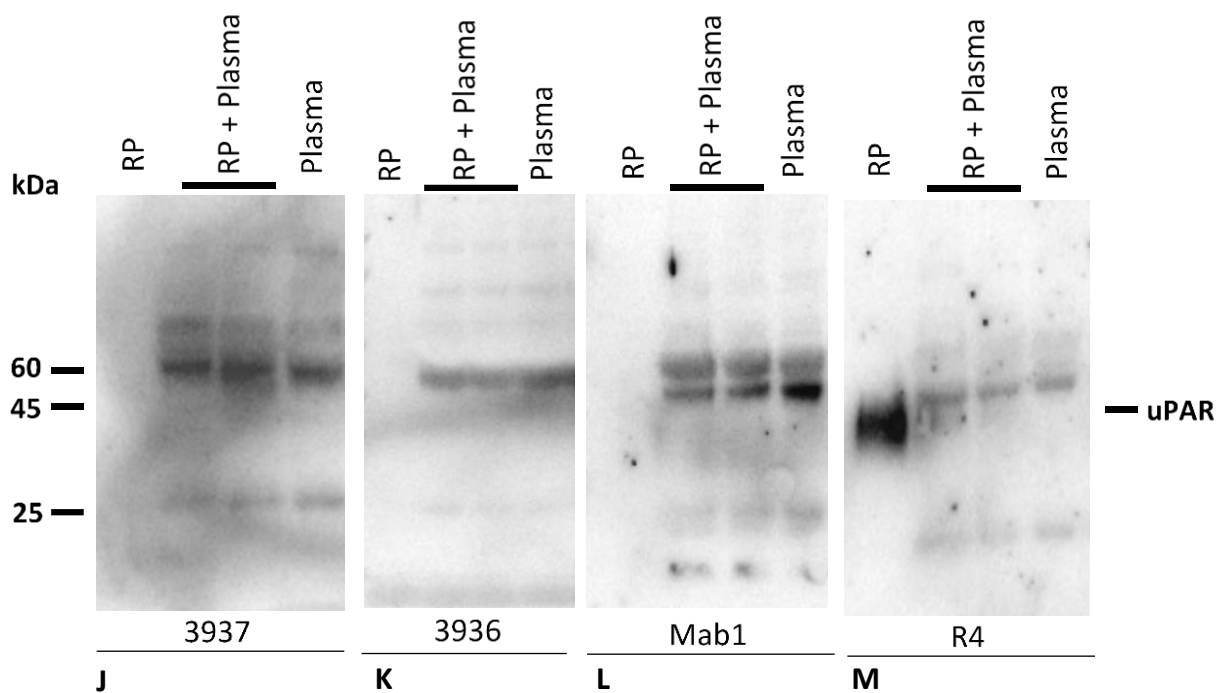


Figure 3. Evaluation of uPAR and $\beta 6$ mAb specificity for its recombinant protein target in plasma. 1ug of recombinant protein (RP), 1ug of RP in 25ug of plasma and 25ug of plasma were probed with $\beta 6$ antibodies 6.3G9 (A), 6.4B4 (B), 7.8B3 (C), 6.2A1 (D), Hu8G6 (E) and Hupo8 (F). And uPAR antibodies 3937 (J), 3936 (K), Mab1 (L) and R4 (M). Plasma was also probed with isotype control antibodies IgG1 (G), IgG2 (H) and secondary antibody (2^o) HRP-Rabbit (I) against mouse IgG.

For an effective IP in the immuno-MRM, the antibody must be highly specific due to the complexity of plasma. WB validation of the mAbs will be useful to guide the latter design of IP experiments. Therefore, all available mAbs were tested by a WB for its specificity in targeting the antigen in a plasma background. This was accomplished by probing the antibodies against the recombinant protein, recombinant protein spiked into plasma and plasma alone. Isotype control antibodies and secondary antibody alone served as controls.

$\beta 6$ mAbs

The $\beta 6$ recombinant protein expected MW under reducing conditions is 110 kDa. Out of the six $\beta 6$ antibodies tested at 1 $\mu\text{g}/\text{mL}$, four appeared to bind to its antigen, showing a band at 100 kDa; 6.4B4 (Figure 3: B), 6.2A1 (Figure 3: D), 7.8B3 (Figure 3: C) and Hupo8 (Figure 3: F). Both 6.3G9 (Figure 3: A) and Hu8G6 (Figure 3: E) did not appear to bind $\beta 6$ (no

band at ~100 kDa). From the four antibodies that showed binding to $\beta 6$ there were three with significantly higher intensity bands: 6.4B4, 6.2A1 and Hupo8. Whilst 7.8B3 appeared to bind $\beta 6$, it was a very weak signal.

All but two antibodies (6.4B4 and Hupo8) had unspecific targets in plasma, which were weak intensity bands visible at the exposure required to detect the $\beta 6$ band. The unspecific targets in plasma were at 60 kDa (7.8B3, Hu8G6 and 6.3G9) and 25 kDa (6.3G9 and 6.2A1).

uPAR mAbs

The uPAR recombinant protein expected MW under reducing conditions is 40-55 kDa. Out of the four antibodies tested at 1 $\mu\text{g}/\text{mL}$, only one, R4, was observed to bind to its antigen, showing a band at 45 kDa (Figure 3:M). Whilst R4 strongly detected recombinant uPAR (1 μg), it did not detect it in a plasma background (25 μg). Antibodies 3937, 3936 and Mab1 did not detect any uPAR recombinant (Figure 3: J-L).

All antibodies had unspecific targets in plasma. These were at 60 kDa, (3937, 3936, Mab1 and R4), 25 kDa (3937, 3936 and Mab1) and 50 kDa (Mab1).

Isotype control mAbs

The isotype control antibodies bound to proteins in plasma at the same MW as the $\beta 6$ and uPAR mAbs. IgG1 (Figure 3: G) and IgG2 (Figure 3:H) bound to proteins in plasma at 60 and 25 kDa similar to bands observed in 7.8B3, 6.3G9, 6.2A1, Hu8Ga, 3936, 3937, Mab1 and R4. Additionally, IgG1 shows some weak binding to a protein in plasma at ~100 kDa. The rabbit anti-mouse IgG secondary antibody (Figure 4: I) bound to a protein in plasma at 60 kDa, similar to the bands observed in the antibodies.

4.1.2. Determining antibody sensitivity

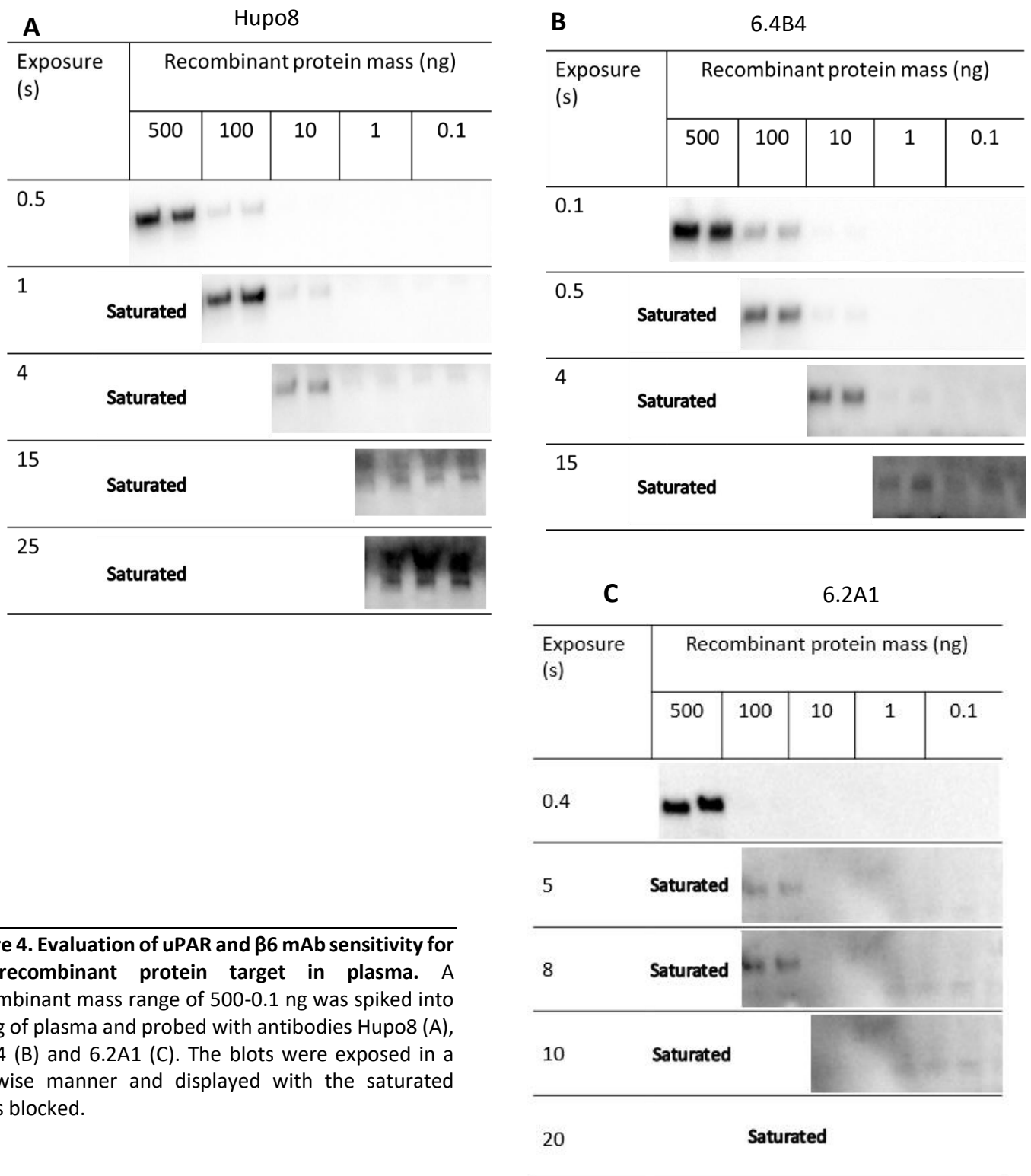
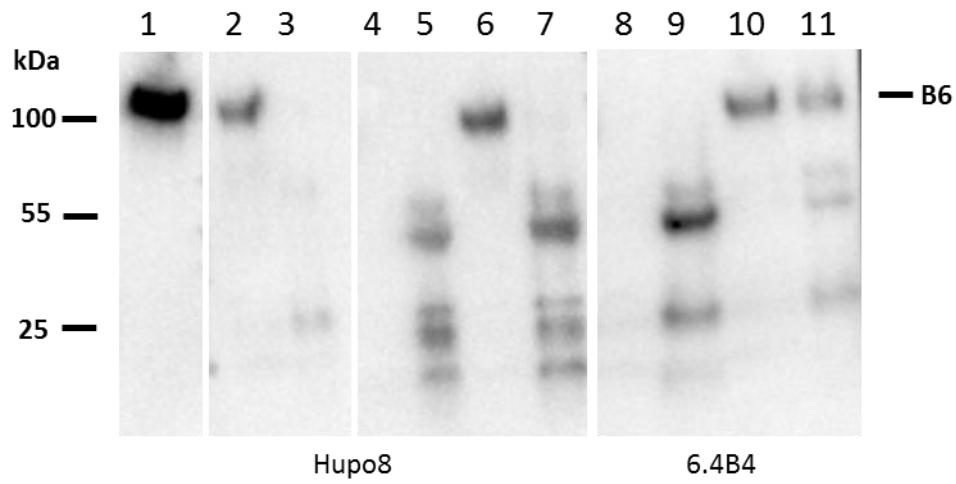


Figure 4. Evaluation of uPAR and $\beta 6$ mAb sensitivity for its recombinant protein target in plasma. A recombinant mass range of 500-0.1 ng was spiked into 25 μ g of plasma and probed with antibodies Hupo8 (A), 6.4B4 (B) and 6.2A1 (C). The blots were exposed in a stepwise manner and displayed with the saturated areas blocked.

Following success in the WB specificity assay, the mAbs were analysed for its sensitivity. This was accomplished by spiking a range of recombinant protein into a constant amount of plasma and assessing the LOD. Blots were exposed in a stepwise manner until the bands became saturated. Images shown here are at the exposure time at which the band became visible to a moderate intensity and before it saturated.

Initially, the blots were exposed to find the highest intensity band and 500 ng of protein was detected at 0.1 sec with 6.4B4 (Figure 4: B), 0.4 sec with 6.2A1 (Figure 4: C) and 0.5 sec with Hupo8 (Figure 4: A). A faint band of 100 ng was also visible with 6.4B4 at 0.1 sec and with Hupo8 at 0.5 sec. The exposure required to clearly see 100 ng was 0.5 sec with 6.4B4, 1 sec with Hupo8 and 5 sec with 6.2A1. To detect 10 ng of protein the blots required exposure to 4 sec with 6.4B4 and 8 sec with Hupo8. Whereas with 6.2A1 increasing exposure (10 and 20 sec) did not detect proteins at 10 ng or lower. At this high exposure very faint bands at a lower MW than $\beta 6$, were visible and were deemed an off-target in plasma. Increasing exposure to 15 sec and 25 sec of the Hupo8 and 6.4B4 blots, respectively, did not reveal any detection lower than 10 ng. There was heavy background fluorescence that saturated both blots. The lowest amount of protein tested and confidently detected by Hupo8 and 6.4B4 was 10 ng, in contrast to the 100 ng LOD with 6.2A1.

4.1.3. Protein A/G magnetic bead immunoprecipitation of recombinant $\beta 6$ protein



1. RP positive control
2. } IP with RP only Supernatant
3. } Eluant
4. } IP with Hupo8 Ab only Supernatant
5. } Eluant
6. } IP with Hupo8 Ab+RP Supernatant
7. } Eluant
8. } IP with 6.4B4 Ab only Supernatant
9. } Eluant
10. } IP with 6.4B4 Ab +RP Supernatant
11. } Eluant

Figure 5. Immunoprecipitation of recombinant $\beta 6$ with antibodies 6.4B4 and Hupo8 using protein A/G beads. 5ug of recombinant protein (RP) was immunoprecipitated with 2ug of mAb and resulting supernatant and eluate was probed on a western blot. There were two negative controls. One was an IP with just RP (no mAb) to observe the proteins stability through the protocol. The second negative control was an IP with just mAb (no RP) to detect the heavy and light chain of the mAb in the eluate. Additionally, a positive control of 1ug RP was included in the WB.

Recombinant protein IP was carried out using two methods, the Pierce Direct IP kit, and protein A/G beads. All IP conducted using the Pierce direct IP kit was unsuccessful. No $\beta 6$ was detected in the elution by a WB. This could be attributed to the chemical cross linking impacting on mAb affinity [90].

The protein A/G protocol contrasted to the Pierce Direct IP in that it did not covalently link the antibody to bead, all incubation was at 4 °C and the antigen incubation was extended to overnight. This preliminary IP was conducted using 5 μg of recombinant $\alpha\beta 6$ and 2 μg of Hupo8 and 6.4B4 mAbs. These antibodies were chosen as they had the best specificity in the WB analysis. Negative control experiments were samples with no recombinant protein and samples with no antibody. A positive control of 1 μg recombinant protein was also included. Each eluate and supernatant was probed on the WB with the same mAb used in the IP. The positive control was probed with Hupo8. Using this protocol 6.4B4 successfully immunoprecipitated recombinant $\beta 6$ protein.

Lane 1 (Figure 5) contains the recombinant positive control and shows the expected $\beta 6$ band at 100 kDa. Lanes 2 and 3 (Figure 5) contain the supernatant and eluate, respectively, from the IP reaction containing only recombinant protein. In lane 2 the supernatant can be seen to have $\beta 6$ as expected. The band is much less intense than the 1 μg lane because only 10 μL (1/50th) of the 500 μL supernatant was taken. In lane 3 the elution has a light band visible at 25 kDa attributed to contamination.

Lanes 4-7 (Figure 5) are from the Hupo8 IP reactions. Lane 4 and 5 are the supernatant and eluate, respectively, from the control IP reaction with Hupo8 mAb and no protein. As expected the supernatant does not have any β . The eluate in lane 5 contains the heavy (H) and light (L) chain of the antibody at 55 and 25 kDa respectively, including any fragments. Lane 6 and 7 are the supernatant and eluate, respectively, from the Hupo8 IP reaction with 2 μg Hupo8 antibody and 5 μg of $\beta 6$ protein. In lane 6 the supernatant which contains any remaining unbound $\beta 6$ shows a $\beta 6$ band at 100 kDa. Indicating $\beta 6$ protein remaining in the supernatant after the IP. The eluate in lane 7, shows the H and L chain of the eluted antibody and no band at the expected $\beta 6$ MW. This indicating no $\beta 6$ in the eluate. The Hupo8 antibody does not successfully capture the recombinant protein in this IP protocol at this concentration.

Lanes 8-11 (Figure 5) are from the 6.4B4 IP reactions. Lane 8 and 9 are the

supernatant and eluate, respectively, from the control IP with 6.4B4 antibody and no protein. This 6.4B4 control IP shows the same protein/band pattern as the Hupo8 control (Figure 5: lane 4 and 5). Lane 10 and 11 are the supernatant and eluate, respectively, from the 6.4B4 IP reaction with 2 μ g antibody and 5 μ g of β 6 protein. The supernatant in lane 10 has a band at 100 kDa, indicating β 6 remaining in the supernatant after the IP. The elution in lane 11 shows the H and L chain of the eluted antibody and additionally a band at the expected β 6 MW. Indicating β 6 recovered in the elution. The 6.4B4 antibody does successfully capture recombinant β 6 protein in this IP protocol at this concentration.

4.2. PRM Mass Spectrometry

4.2.1. uPAR product ion detection and intensity

Table 2. uPAR peptide mass inclusion list for PRM MS analysis

Peptide sequence	<i>m/z</i>	Charge
GNSTHGCSSEETFLIDCR	690.63	3
GPMNQCLVATGTHEPK	870.41	2
CNEGPILELENLPQNGR	651.66	3
YLECISCGSSDMSCER	651.92	3
YLECISCGSSDMSCER	977.38	2
SGCNHPDLDVQYR	520.90	3
LWGGTLLWT	523.79	2
NQSYMVR	449.22	2
LWEEGEELELVEK	801.90	2
SGAAPQPGPAHLSLTITLLMTAR	768.42	3
ITSLTEVVCGLDLCNQGNMGR	1147.05	2
SPEEQCLDVVTH	707.32	2
LGDAFSMNHIDVSCCTK	652.29	3

Table 3. Summary of uPAR transitions detected in recombinant protein

Peptide sequence	# daughter ions obs.	Peak intensity		Top rank ion	Top ranking ion significance
		Min	Max		
GNSTHGCSSEETFLIDCR	7	$1.0 \times 10^5 \pm 1.7 \times 10^5$	$7.3 \times 10^6 \pm 1.0 \times 10^6$	y6+	P=0.03*
CNEGPILELENLPQNGR	9	$5.7 \times 10^7 \pm 1.6 \times 10^7$	$7.8 \times 10^8 \pm 1.6 \times 10^8$	y5+	P=0.03*
YLECISCGSSDMSCER	3	$1.8 \times 10^8 \pm 8.9 \times 10^6$	$5.8 \times 10^8 \pm 3.4 \times 10^8$	y11+	P<0.001**
SGCNHPDLDVQYR	12	$4.0 \times 10^7 \pm 2.1 \times 10^6$	$3.1 \times 10^9 \pm 3.6 \times 10^8$	y8+	P=0.04*
LWEEGEELELVEK	6	1.6×10^7	$6.0 \times 10^8 \pm 7.4 \times 10^7$	Y9+	P=0.02*
LWGGTLLWT	1	$1.8 \times 10^6 \pm 4.0 \times 10^5$		b7+	n/a
GPMNQCLVATGTHEPK	6	$3.5 \times 10^5 \pm 1.2 \times 10^5$	$8.5 \times 10^6 \pm 1.8 \times 10^6$	y9+	ns
SGAAPQPGPAHLSLTITLLMTAR	4	2.3×10^4	$1.6 \times 10^5 \pm 2.9 \times 10^4$	b12	ns
ITSLTEVVCGLDLCNQGNMGR	3	$3.8 \times 10^7 \pm 9.2 \times 10^6$	$2.8 \times 10^8 \pm 6.3 \times 10^7$	y13+	ns
SPEEQCLDVVTH	7	$4.5 \times 10^6 \pm 3.1 \times 10^5$	$1.2 \times 10^7 \pm 1.1 \times 10^6$	y7+	ns

n/a= insufficient data for T-test analysis

The aim of this experiment was to determine the highest intensity daughter ion for each peptide and thus the optimal transitions for uPAR. A complete digest of recombinant protein is expected to yield equal amounts of peptides, therefore differences in peptide intensity in the PRM-MS is due to peptide performance in the MS. Thus, peak intensity was used as a measure of peptide and transition performance [91].

Recombinant protein (100 ng) was digested and analysed in triplicate by LC-PRM-MS on the Q-Exactive on a 1 hour gradient. Representative peaks of each peptide are in figure 6. In the MS collision cell each peptide undergoes fragmentation to produce daughter y- and b-ions which contain the N- and C-termini of the peptide ion, respectively [80]. The average peak area of each daughter ion was compared to determine the highest intensity ion for each peptide, shown here as mean \pm standard error (SEM). Not all peptides were observed in every replicate, therefore some data is derived from a single run and do not contain error bars.

The 10-peptide inclusion list generated from SRMATlas (Table 2) was further

increased by the addition of three peptides detected in plasma from DIA-MS in our group (ITSLTEVVCGLDLCNQGNSGR (1147.05), SPEEQCLDVVTH (707.32) and LGDAFSMNHIDVSCCTK (652.29)¹). Out of the 13-peptide inclusion list, all but NQSYMVR (449.22), YLECISCGSSDMSCER (651.92) and LGDAFSMNHIDVSCCTK (652.29) were consistently detected in the MS analysis discussed here. Of the peptides detected from recombinant uPAR two were located on D1, one in D2, one spanning D2- linker-D3 and five on D3.

The summary data and statistical evaluation is in table 3. The number of detected daughter ions is variable among the peptides, with a range of one to twelve. Peptide SGCNHPDLVDVQYR (520.90), had the most number of daughter ions detected whereas peptide LWGGTLLWT (523.79) only had one daughter ion detected. Daughter ions were ranked from highest intensity to lowest and most peptides had a top ranked daughter ion that's significantly higher relative to others.

Peptides; GNSTHGCSSEETFLIDCR (690.63), CNEGPILELENLPQNGR (651.66), YLECISCGSSDMSCER (977.38), SGCNHPDLVDVQYR (520.90) and LWEEGEELELVEK (801.90) all had top-ranked daughter ions with a higher intensity signal compared to others (Figure 6: A, C, D, E and G). Peptide LWGGTLLWT had one detected daughter ion, b7+ (741.43) and this was considered the highest intensity transition for this peptide (Figure 6: F). Peptides; GPMNQCLVATGTPEPK (870.41), SGAAPQPGPAHLSLTITLLMTAR (768.42), ITSLTEVVCGLDLCNQGNSGR (1147.05) and SPEEQCLDVVTH (707.32) had multiple daughter ions but the top-ranked ion was not statistically significant.

Peptide GPMNQCLVATGTPEPK (870.41) had three top ranked ions, y9+ (939.49), y11+ (1212.60) and y10+ (1052.57), with similar intensities that were significantly higher ($p=0.01^*$) than the fourth ranked ion (Figure 6: B). Peptide SGAAPQPGPAHLSLTITLLMTAR (768.42) had three detected daughter ions of which b4+ (287.14) data is from a single data point, therefore cannot be statistically compared (figure 4:H). Peptide ITSLTEVVCGLDLCNQGNSGR (1147.05) had two top ranked ions, y13+ (1450.62) and y12+ (129.59), with similar intensities that were significantly higher than the third-ranked ion ($p=0.02^*$) (Figure 6: I). Peptide SPEEQCLDVVTH (707.32) had two top intensity ions, y7+ (843.40) and b8+ (959.38), with similar intensities that were significantly higher than the

¹ Peptides are shown as: peptide sequence (m/z) and daughter ions as y- or b-ion (m/z)

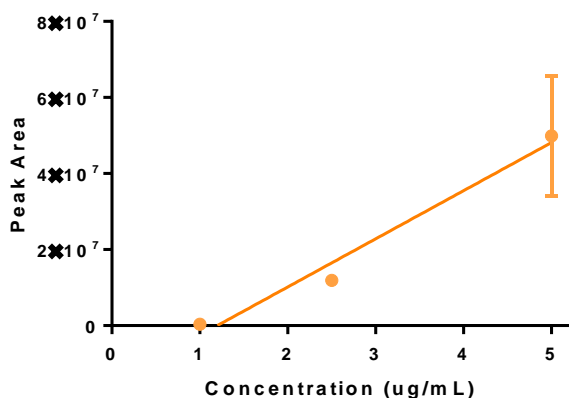
third- ranked ion ($p=0.04^*$). For these four peptides the top-ranked ion was considered the top performing transition.

Majority of all detected ions were singly charged γ -ions (44%) and singly charged b-ions (39%) whereas doubly charged γ (13.8%) and b-ions (3.45%) were a minority. Of all the highest intensity ions across all peptides, 8 out of 10 are singly charged γ -ions and 2 out of 10 are singly charged b-ions.

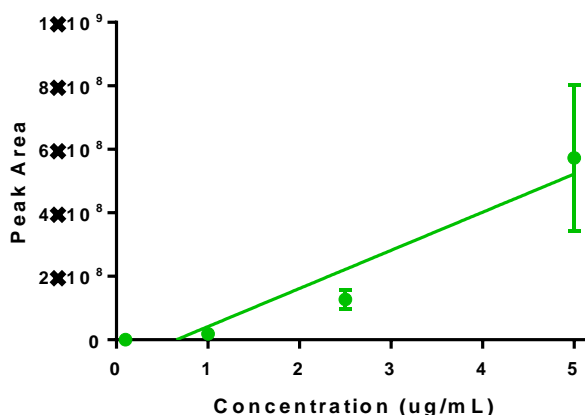
The best transition of each peptide was compared (Figure 6: K). The top- ranked daughter ions had an intensity range of 1.9×10^5 to 3.1×10^9 . A 4-fold difference from the lowest intensity transition, SGAAPQPGPAHLSLTITLLMTAR: $\gamma_{17++}^{(1)}$ to the highest SGCNHPDLVDVQYR: γ_{8+} ($p=0.001^{**}$). The 2nd- 4th ranked transitions (CNEGPILELENLPQNGR: γ_{5+} , LWEEGEELELVEK: γ_{9+} , YLEICISGSSDMSCER: γ_{11+}) were not significantly different. They were however significantly higher than the 5th ranked transitions ($p=0.01^*$). Therefore, there are four uPAR transitions with significant higher intensity compared to other uPAR peptides.

4.2.2. uPAR transition limit of detection

A. GPMNQCLVATGTHEPK: γ_{9+}



B. CNEGPILELENLPQNGR: γ_{5+}



¹ Transitions are shown as: peptide sequence: daughter ion

Table 4. Correlation coefficient of two linear models of uPAR transitions response curve and its limit of detection (LOD).

Transitions	Correlation coefficient		LOD ($\mu\text{g/mL}$)
	Best fit	($x=0, y=0$)	
GPMNQCLVATGTHEPK: $\gamma 9+$	0.976	0.8459	1
CNEGPILELENLPQNGR: $\gamma 5+$	0.92	0.8746	0.1
YLECISCGSSDMSCER: $\gamma 11+$	0.939	0.9287	0.01
SGCNHPDLVDVQYR: $\gamma 8+$	0.9067	0.8881	0.01
LWGGTLLWT: $b 7+$	0.944	0.925	0.1
LWEEGEELELVEK: $\gamma 9+$	0.962	0.9346	0.1
ITSLTEVVCGLDLCNQGNNSGR: $\gamma 13+$	1	0.9254	0.1
SPEEQCLDVVTH: $\gamma 7+$	0.9185	0.88	1

Table 5. Percentage error from two linear models of uPAR transitions response curve

Transitions	Concentration ($\mu\text{g/mL}$)	% error	
		Best fit	($x=0,y=0$)
GPMNQCLVATGTHEPK: $\gamma 9+$	5	-2.72	-15.08
	2.5	14.50	45.03
	1	-22.65	95.66
CNEGPILELENLPQNGR: $\gamma 5+$	5	-8.40	-15.45
	2.5	31.44	48.65
	1	18.97	81.10
	0.1	-555.85	98.03
YLECISCGSSDMSCER: $\gamma 11+$	5	-8.98	-11.60
	2.5	23.06	28.71
	1	-0.35	20.89
	0.1	-186.00	81.94
	0.01	-26834.86	87.51
SGCNHPDLVDVQYR: $\gamma 8+$	5	-11.40	-15.32
	2.5	45.03	55.24
	1	6.55	36.83
	0.1	-266.89	97.09
	0.01	-36336.45	88.25
LWGGTLLWT: $b 7+$	5	-7.16	-10.98
	2.5	30.38	39.95
	1	-7.64	24.17
	0.1	-298.69	70.32
LWEEGEELELVEK: $\gamma 9+$	5	-5.79	-10.30
	2.5	21.64	32.15
	1	13.47	55.76
	0.1	-379.40	92.41
ITSLTEVVCGLDLCNQNSGR: $\gamma 13+$	5	-5.16101	-11.3046
	2.5	27.52538	44.16313
	1	-43.0084	6.597059

The aim of this experiment was to assess the linearity and LOD of uPAR transitions. This was accomplished by analyzing the peak performance in a concentration range of 5, 2.5, 1 and 0.1 $\mu\text{g/mL}$. The samples were run in triplicates and evaluated in the same method as

described above.

Data was analyzed with a two linear regression models to assess the accuracy of correlation between peak intensity and concentration. The highest intensity transition per peptide as determined from the previous experiment is shown as mean \pm SEM and where the error bar is smaller than the size of the symbol it is not shown (Figure 7). The percentage error (expected value-calculated value / expected value) was compared between a best-fit regression curve and one fitted through zero ($x=0, y=0$) (Table 5). The LOD was defined as the lowest concentration point that produced a confident peak.

Two peptides, GNSTHGCSSEETFLIDCR and SGAAPQPGPAHLSLTITLLMTAR, that were detected in the previous experiment was not confidently detected in this experiment. Therefore 8 peptides are described here. The correlation coefficient (R^2) and LOD of each transition is listed in table 4. The average correlation coefficient between peak area and peptide concentration was 0.95 with a best-fit regression and 0.90 when fitted through zero. However, when both models were used to recalculate the concentration from the peak area, on average, there was a relatively large % error (Table 5). This % error has an overall trend of being relatively lower at higher concentrations and higher error at lower concentrations.

An example transition is discussed and all other transitions summarized in table 4. The limit of detection for transition GPMNQCLVATGTHEPK: $y9+$ was 1 $\mu\text{g}/\text{mL}$ (Figure 7: A). A linear best fit had an R^2 value of 0.97, which describes a strong linear relationship between peak area and concentration. A linear curve fitted through zero had a reduced R^2 value of 0.85 (Table 4). The % error analysis showed that a best-fit line was relatively more accurate at modelling higher concentrations than a line forced through zero (Table 5). Whereas a line forced through zero was better at modelling the lower concentrations. This trend in R^2 value difference and % error was observed across all transitions (Table 4 and 5).

Transitions with the strongest linearity as indicated by R^2 values above 0.95 with an autofit are ITSLTEVVCGLDLCNQGNNSGR: $y13+$ ($R^2=1$), GPMNQCLVATGTHEPK: $9+$ ($R^2=0.97$) and LWEEGEELELVEK: $y9+$ ($R^2=0.96$). All other transitions have a R^2 value between 0.90-0.95. Majority of transitions LOD was 0.1 $\mu\text{g}/\text{mL}$ (Table 4). Transitions YLECISCGSSDMSKER: $y11$ and SGCNHPDLVDVQYR: $y8+$ had the lowest LOD of 0.01 $\mu\text{g}/\text{mL}$ whereas GPMNQCLVATGTHEPK: $y9+$ and SPEEQCLDVVTH: $y7+$ had the highest LOD of 1 $\mu\text{g}/\text{mL}$.

Figure 8. Recombinant $\beta 6$ peptides transition detection and intensity in a LC-PRM-MS analysis. 10 $\mu\text{g}/\text{mL}$ of digested recombinant $\beta 6$ was injected into a Q-Exactive Thermo Instrument on PRM mode and analysed via Skyline. The peak area of all daughter ions detected in each peptide was compared by an unpaired T-test to determine the top intensity transition per peptide (A-I). Each peptide highest intensity transitions log10 peak area was compared (J).

Table 7. Summary of $\beta 6$ transitions detected in recombinant protein

Peptide sequence	# daughter ions obs.	Peak intensity		Top rank ion	Top ranking ion significance
		Min	Max		
HILPLTND AER	6	$8.2 \times 10^6 \pm 2.2 \times 10^6$	$6.3 \times 10^7 \pm 1.5 \times 10^7$	b3+	ns
LGFGSFVEKPVSPFVK	8	$2.8 \times 10^5 \pm 2.5 \times 10^5$	$6.6 \times 10^6 \pm 4.4 \times 10^6$	y7+	ns
NSSDIVQIAPQSLILK	1	$2.4 \times 10^4 \pm 6.2 \times 10^3$		y8+	n/a
GCQLNFIENPVSQVEILK	9	$2.1 \times 10^5 \pm 1.6 \times 10^5$	$4.6 \times 10^6 \pm 3.8 \times 10^6$	y7+	ns
VGDTASFSVTVNIPHCER	1	$2.3 \times 10^4 \pm 6.0 \times 10^3$		b13++	n/a
NEYSMSTVLEYPTIGQLIDK	3	$7.5 \times 10^3 \pm 1.4 \times 10^3$	7.6×10^4	y9++	ns
SCIECHLSAAGQAR	7	$2.4 \times 10^8 \pm 2.1 \times 10^5$	$3.0 \times 10^6 \pm 1.1 \times 10^5$	y7+	P=0.03*
WQTGTNPLYR	1	$5.3 \times 10^4 \pm 3.3 \times 10^4$		y7+	n/a
GLLCGGNGDCDCGECVCR	2	$1.1 \times 10^5 \pm 1.2 \times 10^3$	$6.1 \times 10^4 \pm 1.0 \times 10^4$	y6+	P=0.03*

n/a= insufficient data for T-test analysis

The aim of this experiment was to determine the highest intensity daughter ions per peptide and thus the highest intensity transitions for $\beta 6$. The experiment design, analysis and presentation, except being a duplicate set of data instead of a triplicate, is the same as described above (section 4.2.1). The $\beta 6$ 10-peptide inclusion list was generated from SRMAAtlas (Table 6). Out of the 10-peptide list, all but the doubly charged NSSDIVQIAPQSLILK (863.98) peptide was consistently detected in the MS analysis discussed here.

The summary data and statistical evaluation is in table 7. The number of daughter ions detected was variable among the peptides, with a range of one to nine. Peptide GCQLNFIENPVSQVEILK (696.70), had the most number of daughter ions detected whereas peptides NSSDIVQIAPQSLILK (863.98), VGDTASFSVTVNIPHCER (663.66) and WQTGTNPLYR (618.31) only had 1 daughter ion detected (Figure 8: C, D, E & H). Due to the low power of

the study with only a duplicate (due to restricted MS instrumentation time) set of data, many ion comparisons were not significant in an unpaired T-test analysis. Out of the nine peptides, only two, SCIECHLSAAGQAR (520.57) and GLLCGGNGDCDCGECVCR (686.92) had statistically significant top ranked ions (Figure 8: G and I).

Peptides HILPLTND AER (426.90), LGFGSFVEKPVSPFVK (579.99), GCQLNFIENPVSQVEILK (696.70) and NEYSMSTVLEYPTIGQLIDK (767.72) had multiple daughter ions but the top ranked ion intensity was not statistically significant. Peptide HILPLTND AER (426.90) had six detected daughter ions of which the top two ranked ions, b₃⁺ (364.23) and y₅⁺ (604.27), had similar intensities and was significantly higher than the lowest two intensity ions b₄⁺ (461.14) (p=0.04*) and b₅⁺ (574.37) (p=0.04*) (Figure 8: A). The top ranked ion, b₃⁺ was considered the top performing transition for this peptide. Peptide LGFGSFVEKPVSPFVK (579.99) had eight detected daughter ions that were not significantly different. The top ranked ion, y₇⁺ was considered the top performing transition for this peptide (Figure 8: B). Peptide GCQLNFIENPVSQVEILK (696.70) had nine detected daughter ions that were not significantly different. The top ranked ion, y₇⁺, was considered the top performing transition for this peptide (Figure 8: D). Peptide NEYSMSTVLEYPTIGQLIDK (767.72) had 3 detected daughter ions of which the highest intensity ion, y₉⁺⁺ (492.79) was from a single data point, therefore therefore could not be statistically compared. The top ranked ion, y₉⁺⁺, is considered the top performing transition for this peptide (Figure 8: F).

Majority of all detected ions were singly charged y-ions (52%). Whereas there was a similar amount of doubly charged y- (24%) and singly charged b-ions (24%) ions detected with only 3% attributed to doubly charged b-ions. Of all the top ranked ions across all peptides six out of eight were singly charged y-ions, and one each of a singly charged b-ion, doubly charged y-ion and doubly charged b-ion (Table 7).

The best transition of each peptide was compared (Figure 8: J). The top ranked daughter ions had an intensity range of 6.3 x10⁷ to 2.0 x10⁴. A 3-fold difference from the lowest intensity peptide, NSSDIVQIAPQSLILK: y₈⁺ to the highest SCIECHLSAAGQAR: y₇⁺ (p=0.004**). The top two transitions had similar intensities and was significantly higher than the third ranked transitions (p=0.04*). Therefore, there were two significantly high intensity transitions for β₆.

Table 8. The correlation coefficient of two linear models of the β_6 transitions standard curve and its limit of detection (LOD).

Transitions	Correlation coefficient		LOD ($\mu\text{g/mL}$)
	Best fit	($x=0, y=0$)	
HILPLTND AER: b3+	0.8937	0.8759	0.08
LGFGSFVEKPVSPFVK: γ 7+	0.9719	0.9682	0.04
GCQLNFIENPVSQVEILK: γ 7+	0.9168	0.8977	1.25
SCIECHLSAAGQAR: γ 7+	0.9144	0.9096	0.08
GLLCGGNGDCDCGECVCR: γ 6+	0.9846	0.8193	1.25

The aim of this experiment was to assess the limit of detection of β_6 transitions. This experiment was at preliminary stage and thus samples were in singlicate in a concentration range of 5, 2.5, 1.25, 0.08 and 0.04 $\mu\text{g/mL}$. The data analysis and presentation is the same as described above (section 4.2.2), with exceptions noted.

Two peptides, NSSDIVQIAPQSLILK and WQTGTNPLYR, that were detected in the previous experiment was not confidently detected and therefore seven peptides are described here. The correlation coefficient and LOD of each transition are listed in table 8. The average correlation coefficient between peak area and peptide concentration was 0.93 with a best-fit regression and 0.89 when fitted through zero. An analysis of % error was not performed due to the low R^2 values, and preliminary style of the experiment. More repeats are required for the analysis.

Peptide VGDTASFSVTNIPHCER (663.65) was previously detected by single daughter ion b13+, but in this experiment, ion γ 5+ (698.30) was the only one detected and only in concentrations of 5 and 2.5 $\mu\text{g/mL}$ (data not shown). Due to only having two data points, a linear regression is not applied to this transition. Transition NEYSMSTVLEYPTIGQLIDK: γ 9+ was only detected in the 5 $\mu\text{g/mL}$ sample and therefore not further analyzed (data not shown). Therefore only 5 transitions were analysed for linearity and LOD.

An example transition is discussed and all other transitions summarized in table 8. The LOD of transition HILPLTND AER: b3+ was 0.08 $\mu\text{g/mL}$ (Figure 9: A). A linear best fit had a R^2

value of 0.89 and 0.88 when fitted through zero.

Only two out of five transitions had R^2 values above 0.95 with an autofit, LGFGSFVEKPVSPFVK: $\gamma 7+$ ($R^2=0.97$), and GLLCGGNGDCDCGECVCR: $\gamma 6+$ ($R^2=0.98$). All other transitions R^2 values were between 0.89 -0.91. Transition LGFGSFVEKPVSPFVK: $\gamma 7+$ had the lowest LOD of 0.04 $\mu\text{g}/\text{mL}$ whereas GCQLNFIENPVSQVEILK: $\gamma 7+$ and GLLCGGNGDCDCGECVCR: $\gamma 6+$ the highest LOD of 1.25 $\mu\text{g}/\text{mL}$ (Table 8).

4.2.5. uPAR PRM-MS assay validation in HCT116 whole cell lysates

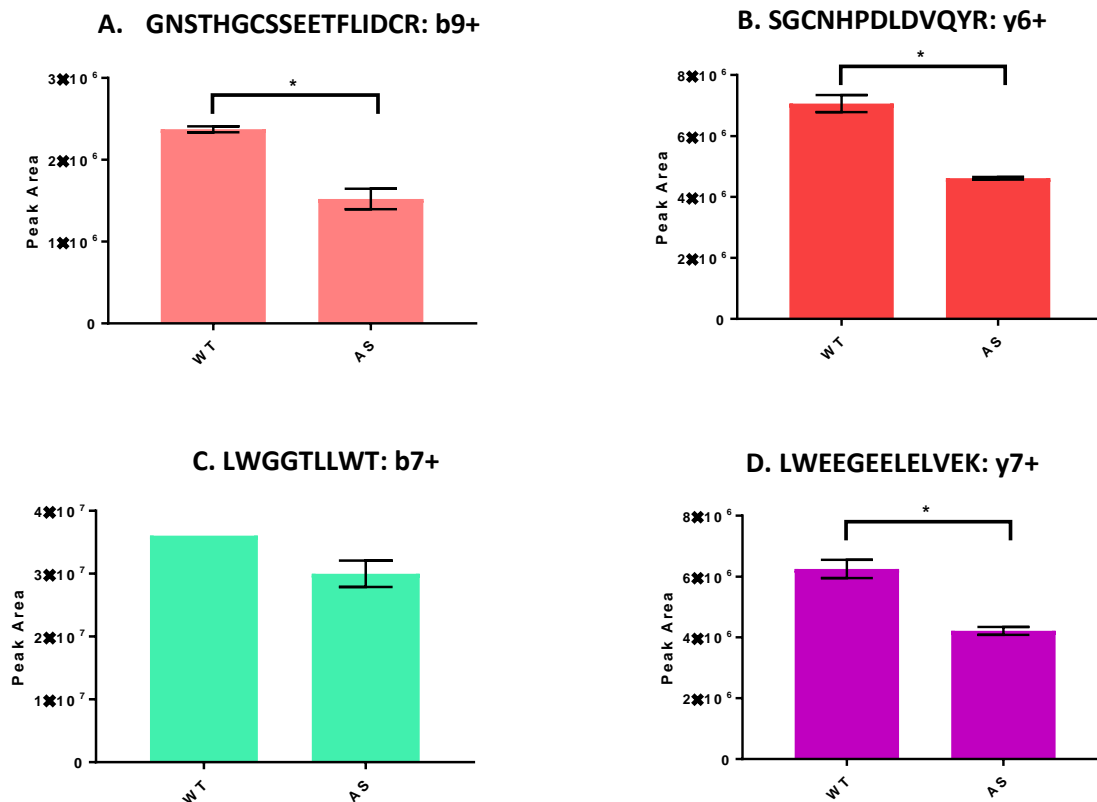


Table 9. uPAR transitions detected in HTCC WT and AS lysate

Transitions		WT	AS	% decrease	Comparison
GNSTHGCSEETFLIDCR	b9+	$2.4 \times 10^6 \pm 3.7 \times 10^4$	$1.5 \times 10^6 \pm 1.2 \times 10^5$	37	P=0.02*
CNEGPILELENLPQNGR	y14+	$2.2 \times 10^7 \pm 9.8 \times 10^5$	$9.9 \times 10^6 \pm 6.5 \times 10^5$	55	P=0.009**
CNEGPILELENLPQNGR	b7++	$8.3 \times 10^6 \pm 2.1 \times 10^6$	$4.7 \times 10^6 \pm 8.6 \times 10^5$	43	P=0.25
CNEGPILELENLPQNGR	b14	$4.6 \times 10^6 \pm 1.6 \times 10^5$	$3.2 \times 10^6 \pm 5.1 \times 10^5$	31	P=0.11
CNEGPILELENLPQNGR	b6+	$3.8 \times 10^6 \pm 3.3 \times 10^5$	$1.6 \times 10^6 \pm 5.2 \times 10^4$	58	P=0.02*
SGCNHPDLDVQYR	y6+	$7.1 \times 10^6 \pm 2.8 \times 10^5$	$4.6 \times 10^6 \pm 4.3 \times 10^4$	34	P=0.01*
LWGGTLLWT	b7+	3.6×10^7	$3.0 \times 10^7 \pm 3.0 \times 10^6$	17	N/A
LWEEGEELELVEK	y7+	$6.3 \times 10^6 \pm 3.0 \times 10^5$	$4.2 \times 10^6 \pm 1.4 \times 10^5$	32	P=0.03*
SGAAPQPGPAHLSLTITLLMTAR	b8+	$4.7 \times 10^6 \pm 3.5 \times 10^5$	$4.0 \times 10^6 \pm 3.7 \times 10^5$	18	P=0.32
SGAAPQPGPAHLSLTITLLMTAR	b4+	$2.3 \times 10^6 \pm 9.0 \times 10^4$	$2.0 \times 10^6 \pm 1.9 \times 10^5$	13	P=0.30

N/A= in sufficient data for T-test analysis.

The aim of this experiment was to test the applicability of the uPAR PRM assay in the CRC derived HCT116 cell line. Furthermore, the sensitivity was also tested by using the AS cell line which has a reported knock down of uPAR protein (Liu et al., 2014).

Ten transitions and six uPAR peptides were detected from the inclusion list (Figure 10, Table 9). Whereas the following five peptides GPMNQCLVATGTHEPK, YLECISCGSSDMSCER, ITSLTEVVCGLDLCNQGNNGR, SPEEQCLDVVTH and LGDAFSMNHIDVSCCTK were not confidently detected in any samples. Location of detected peptides match to all three domains of uPAR; one in each D1, and the linker region D2D3 and four in D3. This indicated the presence of full-length uPAR protein in the HCT116 whole cell lysate. The six peptides detected in the lysate were not the six best performing peptides deemed from the recombinant protein analysis. In fact, the six peptides detected in the lysate were the top three and bottom three performing peptides from the recombinant analysis.

In contrast to the multiple daughter ions per peptide observed in the recombinant analysis in the lysate, all peptides except CNEGPILELENLPQNGR and SGAAPQPGPAHLSLTITLLMTAR were detected by a single daughter ion (Figure 10: E-J, Table 9). All transitions showed the expected reduced intensity in the AS lysate compared to WT, with a reduction range of 13% to 58%. Transition CNEGPILELENLPQNGR: b6+ had the highest reduction of 58% whereas SGAAPQPGPAHLSLTITLLMTAR: b8+ had the lowest of 13% (Table 9). On average, the transitions have a 33.75% decreased intensity in AS cells compared to WT. This decrease in intensity was significant in 5 out of 10 transitions (Table 9).

5. Discussion

CRC can be near curative with surgical resection if detected at early stages [3]. Currently, however, only ~30% of tumours are diagnosed at a stage where surgery can be curative [4]. Majority of diagnosis is at later stages where the tumours have metastasized to local lymph nodes and distal organs, and often toxic chemotherapy is required [5]. There is an urgent clinical need for better diagnostic assays that can be easily deployed as front-line screens and can accurately detect early-stage CRC. This project aimed to fulfill this need by developing a targeted MS assay against two potential early-stage plasma biomarker proteins, uPAR and $\alpha\beta6$. A current state of art MS technique called immuno-MRM. Development of the assay was performed in two phases, (1) affinity based target enrichment and (2) MRM detection. The MRM phase was approached through designing a surrogate PRM assay to determine the best performing peptides and transitions for each protein. Whereas, the affinity assays focused on validating mAbs and developing an IP protocol to effectively capture the target proteins from plasma.

5.1. Affinity assays

The aim of immunoaffinity enrichment is to sensitively and specifically capture native $\alpha\beta6$ and uPAR from plasma and in turn, reduce sample complexity for the following MRM analysis. A highly specific mAb with little or no cross-reactivity is required to ensure low contamination from other plasma proteins in the immunoprecipitation eluate. By reducing sample complexity, the succeeding MRM analysis can more accurately detect and quantify uPAR and $\alpha\beta6$ in plasma because of minimized ion suppression from background matrix components [92]. Sensitive recovery of the target protein is also critical to ensure accurate quantification. Validation of mAbs is necessary to confirm its effectiveness in the immuno-MRM assay. A WB specificity and sensitivity assay is a quick, readily available initial assessment that will serve as a useful tool for latter design of the IP strategy. The samples used in both WB and IP experiments consisted of recombinant protein spiked into healthy control plasma, as a model of CRC plasma. This control plasma was more readily available and cost-effective for assay optimization than diseased plasma. Using this model, antibody specificity and sensitivity in a WB was established and an IP protocol was developed.

5.1.1 Specificity and sensitivity assessment of antibodies

The WB specificity assay revealed that four (6.4B4, Hupo8, 6.2A1 and 7.8B3) out of the five integrin $\beta 6$ antibodies appeared to bind recombinant $\beta 6$ and one (R4) out of four uPAR antibodies appeared to bind recombinant uPAR. In addition to detection of its target epitope, the mAbs cross-reactivity in plasma was also observed.

Interestingly, whilst the anti-uPAR R4 mAb successfully detected 1 μg of recombinant uPAR, it did not detect it in a 25 μg plasma background (Figure 3: M). In this sample, we would expect detection of recombinant uPAR and cross-reactive species, however, only off-target plasma proteins were detected. This could be due to cross-reactivity with higher abundant plasma proteins that compete with the target for binding and/or blocking of the epitope on uPAR by plasma proteins [92]. Therefore, using the R4 mAb to capture recombinant uPAR from plasma in an IP is expected to be challenging.

In fact, the majority (80%) of mAbs tested show cross-reactivity in plasma. Only two out of nine tested mAbs (6.4B4 and Hupo8) showed little to no off-targets in plasma (Figure 3: B & F). However, because these blots were not developed until saturation it cannot be concluded that there is no cross-reactivity at all. Off-target binding can be visible, if the blot was subjected to high exposure. Nonetheless, 6.4B4 and Hupo8 mAbs show a much higher affinity to $\beta 6$ than other plasma proteins. All other mAbs tested, showed cross-reacting plasma proteins at the exposure required to detect the target binding. The detected off-target plasma proteins were, however, always at a lower intensity compared to the target. This indicates a somewhat low specificity of these antibodies to the target antigen in a plasma background. Not unsurprisingly, the isotype control antibodies (IgG1 and IgG2) revealed the same pattern of cross-reactivity seen in the antibodies, indicating the common IgG structure could be responsible for the cross-reactivity in plasma (Figure 3: G & H).

This cross-reactivity of the mAbs is required to be addressed in the ensuing IP strategy design. If the cross-reactivity is due to the IgG component of the mAb it is recommended to first preclear the plasma sample with an IgG isotype antibody to remove the nonspecific proteins that might contaminate the final IP eluate [93].

Following the specificity assay, the mAbs sensitivity in detecting its target in plasma was assessed. Of the three $\beta 6$ antibodies tested, 6.4B4 and Hupo8 had a LOD of 10 ng

whereas 6.2A1 had a LOD of 100 ng. Both LODs are not sufficient to detect endogenous $\beta 6$ in disease plasma using a WB. A SDS-PAGE gel has a general capacity to separate 25 μg of proteins and a 25 μg sample of diseased plasma will contain low pg levels of $\beta 6$ which is beyond the antibody sensitivity [61]. However, the LOD does indicate sufficiency in an IP experiment because as much as 3 mg of plasma can be sampled for a single IP reaction [94] This, much larger sample will likely contain low ng/mL level of $\beta 6$ which is within the sensitivity of the antibodies. The mAb sensitivity, as observed in the WB, shows promise in capturing endogenous $\beta 6$ from diseased CRC plasma.

Future work to determine WB specificity and sensitivity assays can be achieved in two parts. First, further experimentation is required to assess the antibodies that did not work in this experiment. Optimisation of antibody and antigen concentration and troubleshooting different parameters of WBs (i.e., incubation time, exposure settings, and buffer concentration) should be done to achieve detection. Secondly, all other successful antibodies (R4 and 7.8B3) need to be assessed for their sensitivity. Upon completion, the mAbs will be evaluated for their effectiveness in capturing the target in plasma by an IP.

5.1.2. Immunoprecipitation of recombinant protein

The IP component of the assay development is in its preliminary stages. The search for a suitable strategy to capture the $\beta 6$ and uPAR has proven to be challenging. Ultimately recombinant $\beta 6$, was successfully immunoprecipitated, using the 6.4B4 antibody and protein A/G beads, though target recovery was low. This could be attributed to the high amount of antigen (5 μg) used, saturating the antibody (2 μg). Protocol and antigen-antibody concentration optimization could improve this recovery [95]. In the same protocol, the Hupo8 mAbs were not able to capture any $\beta 6$ protein. Whilst both 6.4B4 and Hupo8 mAbs show relatively similar specificity and sensitivity in the WB assay, they do not have similar effectiveness in an IP. This is unsurprising due to the difference of denatured protein detection in WB and native proteins in an IP [96]. Whilst the Hupo8 mAb detected linearized $\beta 6$ on a WB, it could potentially not access the epitope in its soluble form.

The following optimization is required to complete the development of immunoaffinity enrichment: (i) determine antibody capture of target in a plasma background, (ii) establish sensitivity of capture (LOD) in a plasma background, (iii) reduce sample complexity by

preclearing and (iv) test capture efficiency using multiple antibodies to the same target (multiplexing) [97]. Finally, the immunocapture protocol can be streamlined to combine with the LC-MRM-MS analysis to observe transitions and interference.

The almost-complete automation of immunoaffinity enrichment is an advantage of an immuno-MRM. Paulovich and colleagues utilized a KingFisher magnetic bead handling platform, equipped to use 96 well plates, for automated high throughput target enrichment prior to LC-MRM [92]. In this partially automated assay, samples can be processed in ~2.5 hrs following the overnight antigen incubation, reducing operation time by three to four times. We propose a similar automation to be applied to our immunoaffinity enrichment strategy to increase throughput. This will enable dozens of CRC patient samples to be processed in parallel prior to LC-MRM-MS.

5.2. PRM Mass Spectrometry

The immunoaffinity capture will be ultimately combined with the MRM parameters to complete the immuno-MRM assay. The aim of the MRM component is to reliably and reproducibly detect and quantify uPAR and $\beta 6$. The detection is accomplished by using transitions (peptide-daughter mass ion pairs) to program the 1st and 3rd quadrupole of a mass spectrometer to filter only the target peptide and daughter ion of interest. Quantification is by spiking known amounts of a synthetic heavy labelled homolog proteins of the transitions and using the H/L ratio of peptides [68, 70]. Optimal transitions based on peak intensity, linearity and LOD were chosen for each protein as part of this project. This was carried out using the PRM mode on the Q-Exactive Hybrid Quadrupole-Orbitrap MS which does a high-resolution full scan acquisition of all daughter ions. Unlike in a typical MRM where each peptide has a single daughter ion monitored, the Orbitrap on the Q-Exactive detects all daughter ions of each peptide in a single analysis. This method was utilized due to limited MS availability.

5.2.1. $\beta 6$ and uPAR product ion detection and intensity

A complete digest of recombinant protein is expected to produce equimolar peptides and therefore difference in peak intensity (or relative abundance) is due to the peptide performance variability in the MS [91]. Thus, peak intensity was used as a measure of

transition performance. Low-intensity transitions at a high concentration (10 µg/ml in the transition detection experiment) are more likely to be undetectable in a plasma sample with much lower (~ng/mL) target protein [91, 98]. Peptides that produce high ion-current responses and high abundant fragment ions are likely to have the best detection sensitivity [99]. Therefore, all ions detected from each peptide were compared using an unpaired T-test analysis to determine the highest intensity transition for each peptide.

Three tryptic peptides YLECISGSSDMSCER (651.92), NQSYMVR (449.22) and LGDAFSMNHIDVSCCTK (652.29) of recombinant uPAR were never detected by PRM. Equally, the triply charged tryptic peptide NSSDIVQIAPQSLILK (863.98) of recombinant β6 was also never detected. This is not unexpected considering that it is well known that peptides can have varying MS detectability due to varying ionization efficiencies [91]. Additionally, poor chromatography, solubility problems, matrix interference and failure of recovery from digest can all effect the peptides detection [100].

Most peptides have a singular daughter ion with a significantly higher intensity compared to other daughter ions. This indicates there is a clear optimal transition per peptide, that can be targeted to achieve a greater chance of detection. Furthermore, the significant 4-fold and 3-fold difference in transition intensities among the uPAR and β6 peptides respectively, indicates optimizing target transitions could yield significant differences in LOD of the assay.

5.2.2. β6 and uPAR transition limit of detection

The sensitivity (LOD) of the transitions was assessed by determining the linearity and dynamic range of the uPAR and β6 transitions. For the uPAR transitions, a 500-fold concentration range was tested (5 to 0.01 µg/mL) for detection and intensity. Whereas the β6 transitions were assessed at a preliminary level with a 62-fold concentration range (5 to 0.08 µg/mL). Two peptides from each uPAR and β6 that were detected in the previous experiment, were not detected in this LOD experiment. This may be attributed to peptide degradation within the pre-prepared protein digest stock.

Two linear regressions were evaluated for their accuracy in modelling the concentration peak response data: the best-fit line and a line forced through zero. This strategy was employed because of the broad concentration range (500-fold and 62-fold) tested and

because MS standard curves are known to lose linearity at very low and high concentrations [101, 102]. Linear regression constrained zero is not always appropriate at modelling the entire data set [103]. The best fit regression was more accurate at modelling higher concentrations whereas a line forced through zero was more accurate at modelling lower concentrations, evident by a relatively lower % error (Table 4). Therefore, we propose the most the appropriate analysis to be the construction of two standard curves: one each to model the higher and lower concentration range with the most accurate linear regression applied to each curve.

In addition to the two-linear model analysis, their accuracy (% error) of predicting the uPAR concentration from the peak response was also assessed. Both types of linear models showed an average of 8% error (ignoring two outliers) in calculating the peptide concentration. This error is largely attributed to the relatively low correlation coefficient values ($R^2 < 0.99$) and improvement in the correlation would likely lower the error. To accomplish this, experiments are needed to be repeated with increased replicates and with varied concentration points to have more data points on the curve. Furthermore, whilst an accurate linear modelling of the response curve is ideal, in MRM-MS the quantification will ultimately be based on the spiked in heavy peptides. Therefore, the observed LOD is the critical finding in this experiment.

As predicted there was large variability in transitions LOD with a 100-fold and 15-fold difference uPAR and $\beta 6$ respectively (Table 3 & 7). Unexpectedly, the highest intensity transitions did not correlate well with those of lowest LOD, in either protein. A good example of this disparity between intensity and LOD are the uPAR transitions ITSLTEVVCGLDLCNQNSGR: $\gamma 13+$ and LWEEGEELELVEK: $\gamma 9+$. Both transitions had similar intensity at the highest concentration point tested, but the peak response dropped off much faster in ITSLTEVVCGLDLCNQNSGR: $\gamma 13+$ compared to LWEEGEELELVEK: $\gamma 9+$. Therefore LWEEGEELELVEK: $\gamma 9+$ has a relatively lower LOD. This means that transitions with a smaller change in intensity per unit concentration (i.e slope of linear regression) have a lower LOD. Therefore, analysis of peptide performance requires consideration of peak intensity of the daughter ions as well as their relative change of intensity over different concentrations.

5.2.3. Transition evaluation and selection

Considering the aim of the immuno-MRM is to enhance sensitivity to detect and accurately quantify LAPs we chose three transitions for uPAR and $\beta 6$ based upon the largest dynamic range. It is noted that the correlation coefficient (i.e. linearity) was not included in this evaluation because it is susceptible to further experimental optimization (e.g., more repeats and a broader concentration range). The three uPAR transitions are YLEICISCGSSDMSCER: $\gamma 11+$ (977.38/1275.44), SGCNHPDLDVQYR: $\gamma 8+$ (520.90/503.25) and LWEEGEELELVEK: $\gamma 9+$ (801.90/1045.54). The three $\beta 6$ transitions are LGFGSFVEKPVSPFVK: $\gamma 7+$ (579.99/773.46), SCIECHLSAAGQAR: $\gamma 7+$ (520.57/660.34) and HILPLTND AER: $b 3+$ (426.90/364.23).

In addition to the MS evaluation of these transitions, the peptide characteristics of amino acid (aa) length, proteotypicity, number of observations, hydrophobicity and single nucleotide polymorphisms (SNPs) were considered [104]. All peptides are between 12-16 aa in length and have a high number of observations in PeptideAtlas by MS, with a total of 360 times for uPAR and 144 for $\beta 6$. High previous experimental observation is supportive of transition reproducibility. All transition peptides were checked for proteotypicity by using protein BLASTP (Uniprot) and unicity checker (Nextprot¹) and confirmed to be unique to $\beta 6$ or uPAR. Water-soluble peptides are preferred for sample preparation and LC performance [91], therefore peptide hydrophobicity was confirmed to be less than 40%. Two uPAR peptides are reported to have the following SNPs: LWEEGEELELVEK 1st E \rightarrow G (in dbSNP:rs4251813) and SGCNHPDLDVQYR D \rightarrow A (in dbSNP:rs16976608). The presence of these SNPs, in endogenous peptides in plasma will introduce a mass change that would evade detection by the PRM assay. However, the SNPs do not seem to have a high prevalence considering they are both within the top three peptides observed for uPAR. Thus, the three transitions chosen for uPAR and $\beta 6$ fulfill the criteria of detectable signature proteotypic peptides for MRM.

As mentioned above, it is important to choose peptides that have been previously observed in MS/MS as it is known to be detectable. The selection of peptide targets is, in fact, a key consideration that usually arise with the design of PRM/MRM assays [80]. All types of targeted MS (PRM, MRM and SRM) require a defined list of target peptides,

¹www.nextprot.org/viewers/unicity-checker/app/index.html

referred herein as the mass inclusion list. This mass list is programmed into the MS 1st quadrupole and is used to filter the peptides of interest based on their mass. It consists of signature proteotypic peptides and can be developed by in-house DIA experiments, identification from data repositories such as SRMAtlas [105] and MRMAid [106] or in silico computational methods such as OpenMS/TOPP [107]. In this study, SRMAtlas which is an extension of PeptideAtlas was used to generate most of the inclusion list for uPAR and all the β 6 list. However, most of the data in PeptideAtlas regarding β 6 and uPAR are not plasma-derived and instead are mostly from cell lysate and tissue studies. Only two and eleven of the 150 and 141 experimental entries in PeptideAtlas as pertaining to β 6 and uPAR, respectively, seem to be conducted in plasma (PeptideAtlas: RochePlasma Combined, unpublished data). This lack of identification in plasma is likely attributed to its low abundance which evades traditional MS detection. Using a non-plasma based data repository like SRMAtlas to develop an assay for plasma proteins can be problematic. This is because the plasma proteome is likely to contain cleaved proteins which would harbor protein fragments not found in cell lysates or tissue samples [108, 109]. Therefore, using SRMAtlas to select the peptide targets may fail to detect endogenous uPAR and β 6 fragments/peptides in plasma. The best strategy is to include DIA data generated in plasma, and/or create an inclusion list based of all possible proteotypic peptides (above 8 aa in length) by in silico digestion. This would enable a more comprehensive search of the target protein in plasma.

In addition to transition optimization in plasma, the PRM assay designed here needs to be translated to an MRM instrument. In fact, Jaffe and colleagues accomplished this transformation in their proposal to use an LTQ-Orbitrap XL™ Hybrid Ion Trap-Orbitrap (ThermoFisher) instrument as a bridge between biomarker discovery and MRM development in QTRAP 4000 triple quadrupole (Applied Biosystems) [100]. In this method, referred to as accurate inclusion mass screening (AIMS), they use the high-resolution Orbitrap-MS system to confidently detect peptides and fragmented daughter ions to reduce the cost and time required to configure MRM assays. Strikingly, 15 out of the 18 peptides detected in the Orbitrap had suitable MRM assay performance on the 4000 Q Trap, and there was also a high concordance in the fragmentation spectra. Therefore, we expect transitions determined in this analysis to be applicable to the target MRM instrument (i.e. AB Sciex TripleTOF 5600+). The comparable sensitivities of Q-Exactive Orbitrap and

traditional triple quadrupole mass spectrometers ensures no significant deviation in the LOD of the transitions observed here [110].

Future work is required to complete uPAR and $\beta 6$ transition LOD determination. Specifically (i) $\beta 6$ limit of detection experiment needs to be repeated with triplicate samples to allow for statistical validation, (ii) the uPAR transitions with the lowest LOD should be re-identified with an even lower concentration range and (iii) both protein concentrations curves need to be spiked into plasma and analysed for interference. The final experiment with recombinant protein spiked into plasma is important to assess ion suppression and matrix interference for each transition. It is expected that plasma proteins will have severe interference and therefore reduce the LOD. Upon successful completion of this work, heavy labelled homolog proteins of the transitions will be used in a series of quantification evaluation experiments.

5.2.4. The uPAR PRM assay validation in CRC cell lysate

The main limitation in using a direct PRM or MRM assay in a complex sample is because of potential for interference from the background matrix and chemical noise [80]. In a complex background such as plasma or cell lysate, co-eluting peptides with similar mass can result in ion contributions from both species. Furthermore, high abundant peptide fragmentation can also interfere with fragment ion detection [91]. Whilst in an immuno-MRM the preceding IP will reduce sample complexity the MRM needs to still reliably detect the target peptides in a proteome background. Therefore, the HCT116 CRC cell line, known to express uPAR [111], was used to validate detection of endogenous uPAR in a cell lysate background. In addition to providing a background proteome to test, this cell line is CRC derived and therefore presents a tumour model to detect endogenous uPAR.

This experiment had the following aims: (1) determine uPAR recovery in a whole lysate preparation, (2) compare the transitions detected between endogenous uPAR and recombinant protein and (3) test the sensitivity of the PRM assay to detect decreased uPAR expression in the AS cell line.

Firstly, uPAR was confidently detected using ten transitions and six peptides in whole cell lysate of both WT and AS cell lines. The six peptides originate from all three domains indicating the presence of full-length uPAR in the lysate. Therefore, HCT116 whole cell lysate preparation sufficiently recovered membrane-anchored uPAR. Transitions between

endogenous uPAR in the lysate and its recombinant was compared at the peptide and daughter ion level. In contrast to recombinant uPAR PRM analysis, which commonly detected multiple daughter ions per peptide, in the lysate, all but two peptides were detected by a single daughter ion. This indicates variability in peptide fragmentation and/or ion detection. Barsnes et al., corroborates this finding in their global analysis of peptide fragmentation variability (Barsnes et al., 2011). By analyzing the same peptide multiple times on a single instrument under conserved experimental conditions, they confirmed substantial variation in the detection rates and intensity of fragment ions. Therefore, comparative samples need to be processed using extremely conserved experimental conditions and within a single MS analysis. Despite variability in daughter ion detection, the comparison of peptide intensity between the lysate and recombinant uPAR revealed a high preservation in relative intensity. For example, peptide CNEGPILELENLPQNGR is the highest intensity peptide from the recombinant experiments and the second highest intensity peptide from the lysate. Similarity in recombinant and endogenous peptide intensity indicates consistent ionization and behavior in the MS, which validates the use of recombinant proteins in assay optimization.

It is worth noting that not all peptides detected in the recombinant uPAR PRM analysis were detected in the HCT116 cell lysate. This is not unexpected considering a lysate extraction is susceptible to protein loss, degradation and biological variability [112]. It is possible that the undetected peptides of uPAR were either degraded, lost or not recovered in the lysis preparation. Additionally, HCT116 derived uPAR could have endogenous post translational modifications (PTMs) that are not present in the recombinant protein [113], and therefore avoid detection in the mass filtering of the 1st quadrupole. Fortunately, the advantage of MRM/PRM-MS is that the known PTMs and isoforms can be targeted by expanding the peptide selection criterion [98]. Therefore, if necessary, the known uPAR glycosylation variants can be included in the PRM assay design [24].

The uPAR PRM assay developed here is sufficiently sensitive to detect uPAR expression difference between WT and AS HCT116 cells. Comparison of peptide intensity revealed a highly accurate 33% decrease expression in AS cells which aligns with the published protein knock down of 27% [88, 111]. The observed sensitivity of the uPAR PRM assay is promising for its application in plasma considering the sensitivity will be further enhanced by combination to immunoaffinity enrichment. Furthermore, the use of the HCT116 CRC cell

line validates the applicability of the assay to endogenous uPAR from patient tumours.

Following this validation, we propose to study secreted and/or cleaved uPAR from HCT116 cells. Considering the final assay intention to detect and quantify uPAR in plasma it is important to assess peptide detection in the secretome. We expect this will be a highly accurate model of a uPAR expressing patient tumour. For the validation of endogenous $\beta 6$ the $\beta 6$ overexpressing CRC stage B derived SW480 cell line will be used [114]. Peptides detected in these future studies will enable highly targeted transition selection with high potential for translation to CRC patient plasma samples.

5.3. Conclusion

The plasma proteome containing tumour secreted proteins presents a valuable resource to study and develop targeted assays against CRC biomarkers. The biggest challenge in detection and quantification of these biomarkers in plasma is their relatively low abundance (ng/mL) compared to more highly abundant homeostatic proteins (mg/mL). To circumvent this challenge, we proposed to develop a two-step assay that captures the proteins by affinity-based enrichment prior to detection by targeted MRM MS. Assay development for clinical practice is often a time-consuming endeavor. This project completed several important initial requirements for development of an immuno-MRM assay. Particularly, (i) determined specificities and sensitivities of a range of monoclonal antibodies, (ii) established a successful affinity-based enrichment strategy, determined optimal transitions and lastly (iii) validated the uPAR PRM assay in a CRC tumour model. The amalgamation of affinity-based target enrichment and the targeted MS assay will result in highly sensitive, specific and reproducible assays to detect uPAR and $\alpha v\beta 6$ in control and diseased patient plasmas. This immuno-MRM will address the unmet clinical need of early-stage CRC diagnostics.

Reference List

1. Smith, H.W. and C.J. Marshall, *Regulation of cell signalling by uPAR*. Nat Rev Mol Cell Biol, 2010. **11**(1): p. 23-36.
2. Organization, W.H., *World Cancer Report 2014*. Vol. Chapter 1. 2014.
3. Meyerhardt, J.A. and R.J. Mayer, *Systemic therapy for colorectal cancer*. N Engl J Med, 2005. **352**(5): p. 476-87.
4. Siegel, R., C. Desantis, and A. Jemal, *Colorectal cancer statistics, 2014*. CA Cancer J Clin, 2014. **64**(2): p. 104-17.
5. Edwards, B.K., et al., *Annual Report to the Nation on the status of cancer, 1975-2010, featuring prevalence of comorbidity and impact on survival among persons with lung, colorectal, breast, or prostate cancer*. Cancer, 2014. **120**(9): p. 1290-314.
6. Davila, R.E., et al., *ASGE guideline: colorectal cancer screening and surveillance*. Gastrointest Endosc, 2006. **63**(4): p. 546-57.
7. Song, L.-L. and Y.-M. Li, *Current noninvasive tests for colorectal cancer screening: An overview of colorectal cancer screening tests*. World Journal of Gastrointestinal Oncology, 2016. **8**(11): p. 793-800.
8. Whitlock, E.P., et al., *Screening for colorectal cancer: a targeted, updated systematic review for the U.S. Preventive Services Task Force*. Ann Intern Med, 2008. **149**.
9. Center for Disease Control and Prevention. *Colorectal Cancer Incidence and Screening — United States, 2008 and 2010*. 2013 [cited 2017 17 February].
10. Katsiampoura, A. and S. Kopetz, *Clinical Applications of Liquid Biopsies in Gastrointestinal Oncology*. Gastrointestinal Cancer Research : GCR, 2014. **7**(4 Suppl 1): p. S8-S12.
11. *NCI Dictionary of Cancer Terms* [cited 2015 14 June]; Available from: <http://www.cancer.gov/publications/dictionaries/cancer-terms?cdrid=45618>
12. Quyun, C., et al., *Recent patents and advances in genomic biomarker discovery for colorectal cancers*. Recent Pat DNA Gene Seq, 2010. **4**(2): p. 86-93.
13. Su, B.-B., H. Shi, and J. Wan, *Role of serum carcinoembryonic antigen in the detection of colorectal cancer before and after surgical resection*. World Journal of Gastroenterology : WJG, 2012. **18**(17): p. 2121-2126.
14. Sajid, K.M., et al., *Carcinoembryonic antigen (CEA) levels in hookah smokers, cigarette smokers and non-smokers*. J Pak Med Assoc, 2007(0030-9982 (Print)).
15. Hasan, M. and A. Mohieldein, *Association between serum carcinoembryonic antigen level and oxidative stress parameters among diabetic females*. International Journal of Clinical and Experimental Medicine, 2015. **8**(4): p. 6489-6494.
16. Tan, E., et al., *Diagnostic precision of carcinoembryonic antigen in the detection of recurrence of colorectal cancer*. Surg Oncol, 2009. **18**(1): p. 15-24.
17. Minton, J.P., et al., *Results of a 400-patient carcinoembryonic antigen second-look colorectal cancer study*. Cancer, 1985. **55**(6): p. 1284-90.
18. Moertel, C.G., et al., *An evaluation of the carcinoembryonic antigen (CEA) test for monitoring patients with resected colon cancer*. Jama, 1993. **270**(8): p. 943-7.
19. Pedersen, S.K., et al., *Evaluation of an assay for methylated BCAT1 and IKZF1 in plasma for detection of colorectal neoplasia*. BMC Cancer, 2015. **15**(1): p. 654.
20. Young, G.P., et al., *A cross-sectional study comparing a blood test for methylated BCAT1 and IKZF1 tumor-derived DNA with CEA for detection of recurrent colorectal cancer*. Cancer Medicine, 2016. **5**(10): p. 2763-2772.
21. Guinney, J., et al., *The consensus molecular subtypes of colorectal cancer*. Nat Med, 2015. **21**(11): p. 1350-1356.
22. Ahn, S.B., et al., *Characterization of the interaction between heterodimeric alphavbeta6 integrin and urokinase plasminogen activator receptor (uPAR) using functional proteomics*. J Proteome Res, 2014. **13**(12): p. 5956-64.
23. Llinas, P., et al., *Crystal structure of the human urokinase plasminogen activator receptor*

- bound to an antagonist peptide. Embo j*, 2005. **24**(9): p. 1655-63.
24. Ploug, M., et al., *Cellular receptor for urokinase plasminogen activator. Carboxyl-terminal processing and membrane anchoring by glycosyl-phosphatidylinositol. J Biol Chem*, 1991. **266**(3): p. 1926-33.
 25. Nielsen, L.S., et al., *Purification of zymogen to plasminogen activator from human glioblastoma cells by affinity chromatography with monoclonal antibody. Biochemistry*, 1982. **21**(25): p. 6410-5.
 26. Ellis, V., N. Behrendt, and K. Dano, *Plasminogen activation by receptor-bound urokinase. A kinetic study with both cell-associated and isolated receptor. J Biol Chem*, 1991. **266**(19): p. 12752-8.
 27. Carmeliet, P., et al., *Urokinase-generated plasmin activates matrix metalloproteinases during aneurysm formation. Nat Genet*, 1997. **17**(4): p. 439-44.
 28. Estreicher, A., et al., *The receptor for urokinase type plasminogen activator polarizes expression of the protease to the leading edge of migrating monocytes and promotes degradation of enzyme inhibitor complexes. J Cell Biol*, 1990. **111**(2): p. 783-92.
 29. Zhang, G., et al., *Urokinase receptor modulates cellular and angiogenic responses in obstructive nephropathy. J Am Soc Nephrol*, 2003. **14**(5): p. 1234-53.
 30. Houck, K.A., et al., *Dual regulation of vascular endothelial growth factor bioavailability by genetic and proteolytic mechanisms. J Biol Chem*, 1992. **267**(36): p. 26031-7.
 31. Lyons, R.M., et al., *Mechanism of activation of latent recombinant transforming growth factor beta 1 by plasmin. J Cell Biol*, 1990. **110**(4): p. 1361-7.
 32. Uszynski, M., et al., *Urokinase plasminogen activator (uPA) and its receptor (uPAR) in gestational tissues; Measurements and clinical implications. Eur J Obstet Gynecol Reprod Biol*, 2004. **114**(1): p. 54-8.
 33. Romer, J., et al., *The receptor for urokinase-type plasminogen activator is expressed by keratinocytes at the leading edge during re-epithelialization of mouse skin wounds. J Invest Dermatol*, 1994. **102**(4): p. 519-22.
 34. Beschorner, R., et al., *Lesion-associated accumulation of uPAR/CD87- expressing infiltrating granulocytes, activated microglial cells/macrophages and upregulation by endothelial cells following TBI and FCI in humans. Neuropathol Appl Neurobiol*, 2000. **26**(6): p. 522-7.
 35. Pyke, C., et al., *Immunohistochemical detection of the receptor for urokinase plasminogen activator in human colon cancer. Histopathology*, 1994. **24**(2): p. 131-8.
 36. de Bock, C.E. and Y. Wang, *Clinical significance of urokinase-type plasminogen activator receptor (uPAR) expression in cancer. Med Res Rev*, 2004. **24**(1): p. 13-39.
 37. de Geus, S.W., et al., *Prognostic Impact of Urokinase Plasminogen Activator Receptor Expression in Pancreatic Cancer: Malignant Versus Stromal Cells. Biomark Insights*, 2017. **12**: p. 1177271917715443.
 38. Ahn, S.B., et al., *Epithelial and stromal cell urokinase plasminogen activator receptor expression differentially correlates with survival in rectal cancer stages B and C patients. PLoS One*, 2015. **10**(2): p. e0117786.
 39. Wilhelm, O.G., et al., *Cellular glycosylphosphatidylinositol-specific phospholipase D regulates urokinase receptor shedding and cell surface expression. J Cell Physiol*, 1999. **180**(2): p. 225-35.
 40. Høyer-Hansen, G., et al., *Hoyer-Hansen G, Ronne E, Solberg H, Behrendt N, Ploug M, Lund LR, Ellis V, Dano KUrokinase plasminogen activator cleaves its cell surface receptor releasing the ligand-binding domain. J Biol Chem* 267: 18224-18229. Vol. 267. 1992. 18224-9.
 41. Sidenius, N., C.F.M. Sier, and F. Blasi, *Shedding and cleavage of uPAR identification and characterisation of uPAR fragments in vitro and in vivo.pdf. FEBS Letters*, 2000. **475**: p. 52-56.
 42. Mustjoki, S., et al., *Soluble urokinase receptor levels correlate with number of circulating*

- tumor cells in acute myeloid leukemia and decrease rapidly during chemotherapy. *Cancer Res*, 2000. **60**(24): p. 7126-32.
43. Wahlberg, K., G. Hoyer-Hansen, and B. Casslen, *Soluble receptor for urokinase plasminogen activator in both full-length and a cleaved form is present in high concentration in cystic fluid from ovarian cancer*. *Cancer Res*, 1998. **58**(15): p. 3294-8.
 44. Stephens, R.W., et al., *Plasma urokinase receptor levels in patients with colorectal cancer: relationship to prognosis*. *J Natl Cancer Inst*, 1999. **91**(10): p. 869-74.
 45. Lomholt, A.F., et al., *Intact and cleaved forms of the urokinase receptor enhance discrimination of cancer from non-malignant conditions in patients presenting with symptoms related to colorectal cancer*. *British Journal of Cancer*, 2009. **101**(6): p. 992-997.
 46. Wei, Y., et al., *Regulation of integrin function by the urokinase receptor*. *Science*, 1996. **273**(5281): p. 1551-5.
 47. Saldanha, R.G., et al., *Proteomic identification of lynchpin urokinase plasminogen activator receptor protein interactions associated with epithelial cancer malignancy*. *J Proteome Res*, 2007. **6**(3): p. 1016-28.
 48. Sowmya, G., et al., *A site for direct integrin α v β 6.uPAR interaction from structural modelling and docking*. *J Struct Biol*, 2014. **185**(3): p. 327-35.
 49. Breuss, J.M., et al., *Restricted distribution of integrin beta 6 mRNA in primate epithelial tissues*. *J Histochem Cytochem*, 1993. **41**(10): p. 1521-7.
 50. Thomas, G.J., M.L. Nystrom, and J.F. Marshall, *Alphavbeta6 integrin in wound healing and cancer of the oral cavity*. *J Oral Pathol Med*, 2006. **35**(1): p. 1-10.
 51. Bandyopadhyay, A. and S. Raghavan, *Defining the role of integrin α v β 6 in cancer*. *Curr Drug Targets*, 2009. **10**(7): p. 645-652.
 52. Li, X., et al., *Alphavbeta6-Fyn signaling promotes oral cancer progression*. *J Biol Chem*, 2003. **278**(43): p. 41646-53.
 53. Hecht, J.L., et al., *Overexpression of the alphavbeta6 integrin in endometrial cancer*. *Appl Immunohistochem Mol Morphol*, 2008. **16**(6): p. 543-7.
 54. Zhang, Z.Y., et al., *Integrin α v β 6 acts as a prognostic indicator in gastric carcinoma*. *Clin Oncol (R Coll Radiol)*, 2008. **20**(1): p. 61-6.
 55. Bates, R.C., et al., *Transcriptional activation of integrin beta6 during the epithelial-mesenchymal transition defines a novel prognostic indicator of aggressive colon carcinoma*. *J Clin Invest*, 2005. **115**(2): p. 339-47.
 56. Ahn, S.B., et al., *Correlations between integrin α v β 6 expression and clinico-pathological features in stage B and stage C rectal cancer*. *PLoS One*, 2014. **9**(5): p. e97248.
 57. Yang, G.Y., et al., *Integrin α v β 6 mediates the potential for colon cancer cells to colonize in and metastasize to the liver*. *Cancer Sci*, 2008. **99**(5): p. 879-87.
 58. Sheppard, D., *Integrin-mediated activation of latent transforming growth factor beta*. *Cancer Metastasis Rev*, 2005. **24**(3): p. 395-402.
 59. Bristow, R.E., et al., *Altered expression of transforming growth factor-beta ligands and receptors in primary and recurrent ovarian carcinoma*. *Cancer*, 1999. **85**(3): p. 658-68.
 60. Liang, B., et al., *Integrin β 6-targeted immunoliposomes mediate tumor-specific drug delivery and enhance therapeutic efficacy in colon carcinoma*. *Clin Cancer Res*, 2015. **21**(5): p. 1183-95.
 61. Bengs, S., et al., *Integrin α v β 6 (ITGB6) Is a Novel Serum Tumor Marker in Colorectal Cancer (CRC) Patients and Is Associated With Invasion and Metastasis of CRC*, in *American Gastroenterological Association*. 2013.
 62. Rogler, G. and M. Scharl, *INTERGRIN α v β 6 FOR DIAGNOSIS/PROGNOSIS OF COLORECTAL CARCINOMA*. 2014, Google Patents.
 63. Anderson, N.L. and N.G. Anderson, *The Human Plasma Proteome: History, Character, and Diagnostic Prospects*. *Molecular & Cellular Proteomics*, 2002. **1**(11): p. 845-867.
 64. Seibert, V., M.P. Ebert, and T. Buschmann, *Advances in clinical cancer proteomics: SELDI-ToF-mass spectrometry and biomarker discovery*. *Brief Funct Genomic Proteomic*, 2005.

- 4(1): p. 16-26.
65. Garbis, S., G. Lubec, and M. Fountoulakis, *Limitations of current proteomics technologies*. J Chromatogr A, 2005. **1077**(1): p. 1-18.
 66. Pieper, R., et al., *Multi-component immunoaffinity subtraction chromatography: An innovative step towards a comprehensive survey of the human plasma proteome*. PROTEOMICS, 2003. **3**(4): p. 422-432.
 67. Anderson, N.L., et al., *Mass Spectrometric Quantitation of Peptides and Proteins Using Stable Isotope Standards and Capture by Anti-Peptide Antibodies (SISCAPA)*. Journal of Proteome Research, 2004. **3**(2): p. 235-244.
 68. Gallien, S., E. Duriez, and B. Domon, *Selected reaction monitoring applied to proteomics*. J Mass Spectrom, 2011. **46**(3): p. 298-312.
 69. Barnidge, D.R., et al., *Absolute quantification of the model biomarker prostate-specific antigen in serum by LC-MS/MS using protein cleavage and isotope dilution mass spectrometry*. J Proteome Res, 2004. **3**(3): p. 644-52.
 70. Anderson, L. and C.L. Hunter, *Quantitative mass spectrometric multiple reaction monitoring assays for major plasma proteins*. Mol Cell Proteomics, 2006. **5**(4): p. 573-88.
 71. Uhlen, M., et al., *A proposal for validation of antibodies*. Nat Methods, 2016. **13**(10): p. 823-7.
 72. Addona, T.A., et al., *Multi-site assessment of the precision and reproducibility of multiple reaction monitoring-based measurements of proteins in plasma*. Nat Biotechnol, 2009. **27**(7): p. 633-41.
 73. Malmstrom, J., et al., *Proteome-wide cellular protein concentrations of the human pathogen Leptospira interrogans*. Nature, 2009. **460**(7256): p. 762-5.
 74. Kuhn, E., et al., *Developing multiplexed assays for troponin I and interleukin-33 in plasma by peptide immunoaffinity enrichment and targeted mass spectrometry*. Clin Chem, 2009. **55**(6): p. 1108-17.
 75. Schoenherr, R.M., et al., *Multiplexed quantification of estrogen receptor and HER2/Neu in tissue and cell lysates by peptide immunoaffinity enrichment mass spectrometry*. Proteomics, 2012. **12**(8): p. 1253-60.
 76. van den Broek, I., et al., *Quantification of serum apolipoproteins A-I and B-100 in clinical samples using an automated SISCAPA-MALDI-TOF-MS workflow*. Methods, 2015. **81**: p. 74-85.
 77. Ahn, Y.H., et al., *Quantitative analysis of an aberrant glycoform of TIMP1 from colon cancer serum by L-PHA-enrichment and SISCAPA with MRM mass spectrometry*. J Proteome Res, 2009. **8**(9): p. 4216-24.
 78. Neubert, H., J. Gale, and D. Muirhead, *Online high-flow peptide immunoaffinity enrichment and nanoflow LC-MS/MS: assay development for total salivary pepsin/pepsinogen*. Clin Chem, 2010. **56**(9): p. 1413-23.
 79. Jung, S., et al., *Quantification of ATP7B Protein in Dried Blood Spots by Peptide Immuno-SRM as a Potential Screen for Wilson's Disease*. J Proteome Res, 2017. **16**(2): p. 862-871.
 80. Liebler, D.C. and L.J. Zimmerman, *Targeted Quantitation of Proteins by Mass Spectrometry*. Biochemistry, 2013. **52**(22): p. 3797-3806.
 81. Whiteaker, J.R., et al., *Sequential Multiplexed Analyte Quantification Using Peptide Immunoaffinity Enrichment Coupled to Mass Spectrometry*. Molecular & Cellular Proteomics : MCP, 2012. **11**(6): p. M111.015347.
 82. Kuhn, E., et al., *Interlaboratory evaluation of automated, multiplexed peptide immunoaffinity enrichment coupled to multiple reaction monitoring mass spectrometry for quantifying proteins in plasma*. Mol Cell Proteomics, 2012. **11**(6): p. M111 013854.
 83. Parker, C.E., et al., *Mass spectrometry in high-throughput clinical biomarker assays: multiple reaction monitoring*. Top Curr Chem, 2014. **336**: p. 117-37.
 84. Peterson, A.C., et al., *Parallel reaction monitoring for high resolution and high mass accuracy quantitative, targeted proteomics*. Mol Cell Proteomics, 2012. **11**(11): p. 1475-88.

85. Weinreb, P.H., et al., *Function-blocking Integrin α v β 6 Monoclonal Antibodies: DISTINCT LIGAND-MIMETIC AND NONLIGAND-MIMETIC CLASSES*. Journal of Biological Chemistry, 2004. **279**(17): p. 17875-17887.
86. Romero-Calvo, I., et al., *Reversible Ponceau staining as a loading control alternative to actin in Western blots*. Analytical Biochemistry, 2010. **401**(2): p. 318-320.
87. Reader, P.P. and A.M. Shaw, *Kinetic Analysis of the Multivalent Ligand Binding Interaction between Protein A/G and IgG: A Standard System Setting*. J Phys Chem B, 2017. **121**(38): p. 8919-8925.
88. Liu, X., et al., *Urokinase-type plasminogen activator receptor regulates apoptotic sensitivity of colon cancer HCT116 cell line to TRAIL via JNK-p53 pathway*. Apoptosis, 2014. **19**(10): p. 1532-1544.
89. MacLean, B., et al., *Skyline: an open source document editor for creating and analyzing targeted proteomics experiments*. Bioinformatics, 2010. **26**(7): p. 966-8.
90. Sousa, M.M.L., et al., *Antibody cross-linking and target elution protocols used for immunoprecipitation significantly modulate signal-to noise ratio in downstream 2D-PAGE analysis*. Proteome Science, 2011. **9**: p. 45-45.
91. Keshishian, H., et al., *Quantitative, multiplexed assays for low abundance proteins in plasma by targeted mass spectrometry and stable isotope dilution*. Mol Cell Proteomics, 2007. **6**(12): p. 2212-29.
92. Whiteaker, J.R., et al., *An automated and multiplexed method for high throughput peptide immunoaffinity enrichment and multiple reaction monitoring mass spectrometry-based quantification of protein biomarkers*. Mol Cell Proteomics, 2010. **9**(1): p. 184-96.
93. Harlow, E. and D. Lane, *Immunoprecipitation: preclearing the lysate*. CSH Protoc, 2006. **2006**(4).
94. Lin, D., et al., *Comparison of Protein Immunoprecipitation-Multiple Reaction Monitoring with ELISA for Assay of Biomarker Candidates in Plasma*. Journal of Proteome Research, 2013. **12**(12): p. 5996-6003.
95. Marcon, E., et al., *Assessment of a method to characterize antibody selectivity and specificity for use in immunoprecipitation*. Nat Meth, 2015. **12**(8): p. 725-731.
96. Trieu, E.P., J.K. Gross, and I.N. Targoff, *Immunoprecipitation-Western Blot for Proteins of Low Abundance*, in *Protein Blotting and Detection: Methods and Protocols*, B.T. Kurien and R.H. Scofield, Editors. 2009, Humana Press: Totowa, NJ. p. 259-275.
97. Nicol, G.R., et al., *Use of an immunoaffinity-mass spectrometry-based approach for the quantification of protein biomarkers from serum samples of lung cancer patients*. Mol Cell Proteomics, 2008. **7**(10): p. 1974-82.
98. Liu, X., et al., *Constrained Selected Reaction Monitoring: Quantification of selected post-translational modifications and protein isoforms*. Methods (San Diego, Calif.), 2013. **61**(3): p. 304-312.
99. Fusaro, V.A., et al., *Prediction of high-responding peptides for targeted protein assays by mass spectrometry*. Nature biotechnology, 2009. **27**(2): p. 190-198.
100. Jaffe, J.D., et al., *Accurate Inclusion Mass Screening: A Bridge from Unbiased Discovery to Targeted Assay Development for Biomarker Verification*. Molecular & Cellular Proteomics : MCP, 2008. **7**(10): p. 1952-1962.
101. Tang, K., J.S. Page, and R.D. Smith, *Charge Competition and the Linear Dynamic Range of Detection in Electrospray Ionization Mass Spectrometry*. Journal of the American Society for Mass Spectrometry, 2004. **15**(10): p. 1416-1423.
102. Tang, L. and P. Kebarle, *Dependence of ion intensity in electrospray mass spectrometry on the concentration of the analytes in the electrosprayed solution*. Analytical Chemistry, 1993. **65**(24): p. 3654-3668.
103. Boyd, R.K., C. Basic, and R.A. Bethem, *Tools of the Trade VII: Statistics of Calibration, Measurement and Sampling*, in *Trace Quantitative Analysis by Mass Spectrometry*. 2008, John Wiley & Sons, Ltd. p. 373-459.

104. Uchida, Y., et al., *A study protocol for quantitative targeted absolute proteomics (QTAP) by LC-MS/MS: application for inter-strain differences in protein expression levels of transporters, receptors, claudin-5, and marker proteins at the blood–brain barrier in ddY, FVB, and C57BL/6J mice*. *Fluids and Barriers of the CNS*, 2013. **10**: p. 21-21.
105. Kusebauch, U., et al., *Using PeptideAtlas, SRMAtlas and PASSEL – Comprehensive Resources for discovery and targeted proteomics*. *Current protocols in bioinformatics / editorial board, Andreas D. Baxevanis ... [et al.]*, 2014. **46**: p. 13.25.1-13.25.28.
106. Mead, J.A., et al., *MRMaid, the web-based tool for designing multiple reaction monitoring (MRM) transitions*. *Mol Cell Proteomics*, 2009. **8**(4): p. 696-705.
107. Nahnsen, S. and O. Kohlbacher, *In silico design of targeted SRM-based experiments*. *BMC Bioinformatics*, 2012. **13**(16): p. S8.
108. Gulcicek, E.E., et al., *Proteomics and the Analysis of Proteomic Data: An Overview of Current Protein-Profiling Technologies*. *Current protocols in bioinformatics / editorial board, Andreas D. Baxevanis ... [et al.]*, 2005. **0 13**: p. 10.1002/0471250953.bi1301s10.
109. Ayache, S., et al., *Comparison of proteomic profiles of serum, plasma, and modified media supplements used for cell culture and expansion*. *Journal of Translational Medicine*, 2006. **4**: p. 40-40.
110. Fedorova, G., et al., *Comparison of the quantitative performance of a Q-Exactive high-resolution mass spectrometer with that of a triple quadrupole tandem mass spectrometer for the analysis of illicit drugs in wastewater*. *Rapid Commun Mass Spectrom*, 2013. **27**(15): p. 1751-62.
111. Ahmed, N., et al., *Proteomic profiling of proteins associated with urokinase plasminogen activator receptor in a colon cancer cell line using an antisense approach*. *PROTEOMICS*, 2003. **3**(3): p. 288-298.
112. Feist, P. and A.B. Hummon, *Proteomic Challenges: Sample Preparation Techniques for Microgram-Quantity Protein Analysis from Biological Samples*. *International Journal of Molecular Sciences*, 2015. **16**(2): p. 3537-3563.
113. Hoofnagle, A.N. and M.H. Wener, *The Fundamental Flaws of Immunoassays and Potential Solutions Using Tandem Mass Spectrometry*. *Journal of immunological methods*, 2009. **347**(1-2): p. 3-11.
114. Niu, J., et al., *Integrin expression in colon cancer cells is regulated by the cytoplasmic domain of the $\beta 6$ integrin subunit*. *International Journal of Cancer*, 2002. **99**(4): p. 529-537.